PREVENTION OF HIP FRACTURES IN ELDERLY PATIENTS USING A PROTECTIVE GARMENT INCORPORATING A SHEAR THICKENING FLUID

by

David Eitan Barlaz

A thesis submitted to the Faculty of the University of Delaware in partial fulfillment of the requirements for the degree of Honors Degree in Chemical Engineering with Distinction.

Spring 2010

PREVENTION OF HIP FRACTURES IN ELDERLY PATIENTS USING A PROTECTIVE GARMENT INCORPORATING A SHEAR THICKENING FLUID

by

David Eitan Barlaz

Approved: _____

Norman J. Wagner, Ph.D. Chemical Engineering
Professor in charge of thesis on behalf of the Advisory Committee

Approved: _____

Charles B. Swanik, Ph.D.
Committee member from the Department of Health, Nutrition, and Exercise Sciences

Approved: _____

Norbert Mulders, Ph.D.
Committee member from the Board of Senior Thesis Readers

Approved: _____

Alan Fox, Ph.D.
Director, University Honors Program

ACKNOWLEDGMENTS

I would like to acknowledge my advisers, Dr. Wagner and Dr. Swanik, and all members of the Wagner and Swanik research groups for their assistance to my research.

From the Wagner lab, I would like to especially thank Dr. Richard Dombrowski for individual advisement and guidance on this project, as well as training on the Instron machine, STF preparation and experimental design. Best of luck on your continued STF research. I would like to thank James McGovern for countless useful discussions related to STF preparation, Matlab simulations, and other topics. You will be sorely missed following our graduation.

From the Swanik research group, I would like to especially thank Dr. Stephen Thomas and Alan Needle for assistance programming for the pendulum impact device and for help with testing. Best of luck to Steve in his post-doc fellowship at UPenn, and the same to Alan currently working on his Ph.D here at UD.

Thanks to John Thiravong at the Center for Composite Materials for help training and for help repairing the drop tower countless times. Thanks to George Whitmyre for training and useful discussions regarding foam work.

Thanks to all my friends and family who have helped me reach this stage for their encouragement and continued support. A special thanks to the entire senior class in the chemical engineering department.

Last but not least, thanks to the Undergraduate Research Program for funding and support.

TABLE OF CONTENTS

LIST OF TABLES

LIST OF FIGURES

ABSTRACT

Fall induced hip fractures are a common form of injury among the elderly. On average, people over 65 years of age suffer at least one fall each year. Possible results include permanent loss of mobility and quality of life if the bone heals or death if complications ensue. Hip fractures are expected to become increasingly common as the current baby boomer generation reaches their later years. Current garments intended to prevent hip fractures, often made of foam, are largely ineffective and are often accompanied by low patient compliance due to comfort and aesthetic issues. Incorporation of a shear thickening fluid (STF) into a protective garment may improve performance because of the large amount of energy dissipated by viscous effects during flow, while providing a solution to some of the comfort issues surrounding patient compliance.

A number of STFs were impact tested using an Instron drop tower to determine their viability in a garment designed for hip fracture prevention. Discontinuously thickening STFs, notably a dispersion of 45 volume % low polydispersity silica nanoparticles in M_W=200 polyethylene glycol, were found to be the best candidates. This specific suspension was chosen over similar candidates due to lower cost of materials. This was due to the peak force experienced by the suspension during impact exhibiting low sensitivity to changes in energy. For a four fold increase in energy, peak force increased less than two fold in this suspension, while it increased as much as six fold for other fluids. All samples exhibited similar sensitivity to variation in sample height.

Squeeze flow simulations of Newtonian fluids were developed in parallel with the drop tower experiments. The inertial effect of the fluid was found to be minimal, thus simplifying future simulations. The effect of the foam casing used was also found to be negligible provided its Young's modulus was less than 1 MPa.

The STF/foam composites were fabricated by loading STF in columns at a variety of area fractions by varying column diameter and holding column spacing constant. Good performance at lower area fractions aids significantly in garment design making the pad more flexible, more lightweight, and cheaper. Performance was found to peak at an area fraction of approximately 0.50. This result was found on both the linear motion impact of the drop tower, as well as the rotational motion of the pendulum impact device. The rotational motion impact decreased peak forces up to an order of magnitude from the linear experiment, the best performing samples had peak forces of about 1.5 kN. Although increased area fraction did not significantly reduce peak force, it did reduce variability in the peak force.

Chapter 1

THE NEED FOR IMPROVED PERFORMANCE OF PROTECTIVE GARMENTS FOR THE PREVENTION OF HIP FRACTURES

1.1 Hip fractures

One of the greatest upcoming challenges for the health care industry in the next decade will be keeping up with the rapid increase in demand for various services as the baby-boomer generation begins to reach old age and retire. Injuries common in the current elderly population will no doubt continue to rise in frequency as the number of people with age associated risk factors continues to grow. Injuries associated with falls are already recognized as a major concern to the elderly. During a fall, a number of injuries can result. Bone density and strength decrease rapidly with age, especially in post-menopausal women, which makes the probability of a broken bone much higher [1]. Other risk factors pertaining to bone density include lifestyle and eating habits including certain medications, smoking, alcohol, and diets low in calcium and vitamin D [2]. If the bone is located in the leg or pelvis, one of the common results is that the displaced bone will damage the tissue and organs around it. Internal organ damage can lead to death directly. Additionally, these types of injuries often require long stays in hospitals and other disability clinics. This increases the risk of contracting a secondary infection, which is also a common cause of death regardless of patient age [1].

Hip fractures are typically in reference to a fractured femur as it is one of the most common bones broken during a fall. Hip fractures are already common among the elderly, with an average of one in three people over the age of 65 falling each year leading to over 15,000 deaths [1]. For those who do survive the fall, the costs to the patient and the medical industry are significant and increasing fast. The cost to the health care industry in 2000 was over $19 billion, and is expected to reach $54.9 billion by 2020. The average cost to an individual, excluding doctor's services is close to $20,000 [3].

Although the mechanics of a human impact and hip fracture are complex, there is a recurring trend in so far as the location of the injury itself. The majority of fractures occur in the femoral neck and the greater trochanter [2]. As seen in Figure 1, the femoral neck is a narrow section of bone which connects the diaphysis (shaft) of the femur to the hip joint itself [4]. The greater trochanter is attached to the femoral neck, and is the most likely point of impact for the femur during a fall.

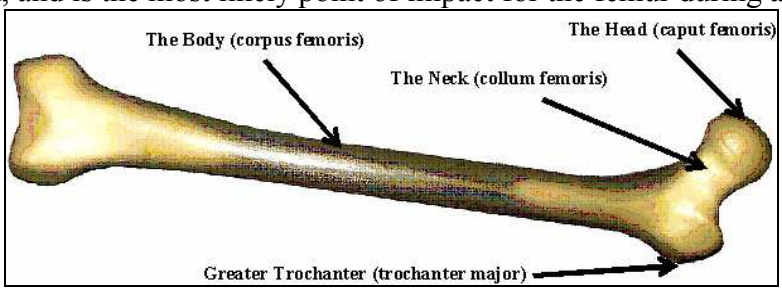

Figure 1: Anatomy of a femur

Because of the danger that hip fractures impose to elderly patients, and the significant costs to the person and the health care industry, hip fractures are a situation in which preventative medicine may have a great deal to offer. Lifestyle changes such as load bearing exercises and diet choices can be effective at decreasing the likelihood of a fall related injury. Fall frequency can be reduced by the installation of hand rails;

this method can be expensive and is not feasible in many situations. Because not all falls are preventable, the need for protective garments is a necessity.

1.2 Protective garments

The types of protective garments currently on the market vary widely in design. Two common types are shown in Figure 2 and Figure 3. Figure 2 shows the HIProtector® HipGuard™ and Figure 3 shows the HIProtector® SAFEHIP®. Garment pictures originally taken by Richard Herseim [4].

Figure 2: Belt type – HipGuard™

Figure 3: Undergarment – SAFEHIP ®

The former is designed to be worn as a belt on top of garments. The belt is several inches thick making it bulky and difficult to wear. The later is much thinner and is designed to be worn as an undergarment. Exact dimensions were not available on the respective manufacturer's websites. While the later of the two garments may be significantly easier to wear, bulges under the clothing are considered by users to be unattractive, and its decreased thickness leads to diminished performance [4]. Both of these garments were among those tested by Richard Herseim, former University of Delaware senior thesis student whose work also dealt with hip fractures. The pads improved performance (reduced peak force) over soft tissue alone by approximately 10-20% [4].

Another design is one proposed by Rabinovitch *et al*. in which the pad is in the shape of an inverted "U" and is worn surrounding the upper region of the femur as seen in Figure 4 [5].

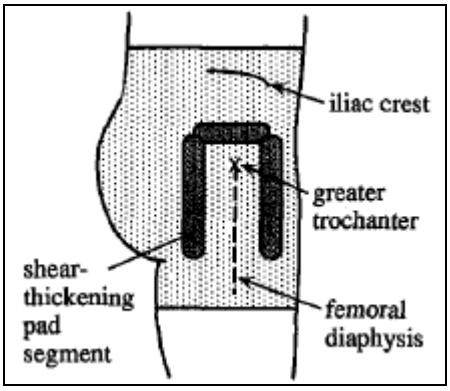

Figure 4: Energy shunting pad

The pad shunts energy away from the hip and into the soft tissue around the stomach and buttocks rather than absorbing the energy of the fall like a traditional pad [5]. Other energy shunting pads are available commercially, but they depend more on proper position of the pad than traditional designs.

The three types of garments shown above are among dozens of with similar designs available on the market today. However, previous work on the efficacy of these protective garments has produced very few encouraging results with regards to efficacy [6-7].

Regardless of which pad a health care professional recommends, patient compliance is continuously low because of discomfort while wearing the pad, mobility issues due to its size or weight, as well as simple issues of aesthetics and ease of use [8-9]. At present, the bulk of garments on the market use foam or rubber as the primary protective material. Rather than relying on these traditional materials, the unique mechanical properties of certain shear thickening fluids may allow for improvement in garment performance in regards to peak force. These fluids show great resistance to flow under shear due to solid like properties. One benefit is that a significant amount energy can be dissipated viscously by the fluid, reducing the peak force during an impact. Another advantage of a fluid is that the garment will be more

flexible than one constructed from foam. One potential drawback of the fluid is that because of its solid like mechanical properties, force may be transmitted across the fluid more easily than with other fluids. Other drawbacks include the weight of the fluid with a density slightly greater than that of water and much greater than most commercial foams or rubbers.

1.3 Shear thickening fluids

A shear thickening fluid (STF) is a highly concentrated colloidal suspension that exhibits non-Newtonian behavior at high stresses/shear rates. When experiencing low shear rates, suspended particles will begin to flow in the direction of the shear; the result is a decrease in viscosity. At a critical shear rate, the particles overcome the weak electrostatic repulsion forces, allowing hydrodynamic lubrication forces to cause particles to be moved closer together forming hydroclusters [10]. The lubrication forces are the result of viscous forces in the thin fluid layers separating the particles. The formation of these clusters causes an increase in the viscosity of the fluid. For all STFs discussed here, the transition is reversible, and the fluid will return to its zero-shear viscosity after deformation ceases. A cartoon of the shear thickening process can be seen in Figure 5 [11].

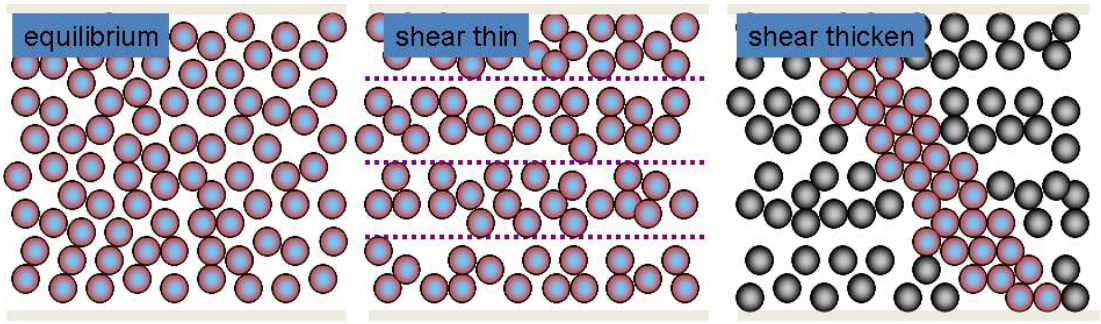

Figure 5: Hydrocluster mechanism of reversible shear thickening

Among the benefits of STFs is that the thickening properties are tunable to suit an individual application using several methods. The relative intensity of the thickening response is dependent on a number of material properties within the suspension including particle-solvent interactions, particle size and polydispersity, and the volume fraction of the particles. If the viscosity versus shear rate curve for a mixture does not make a sudden jump to higher viscosities beyond the critical shear rate, the mixture is said to be continuously shear thickening. If the curve makes a sharp, nearly vertical, increase past the critical shear rate than the mixture is considered discontinuously shear thickening [10]. Figure 6 shows rheology data of highly monodispersed silica particles (diameter = 450 ± 5 nm) in M_W=200 polyethylene glycol from Egres [12]. At low volume fractions, the shear-thickening is continuous, meaning the viscosity v. shear rate curve has a non-vertical slope. As volume fraction increases, the critical shear rate decreases due to the increased frequency of particle collisions, and the thickening response becomes discontinuous.

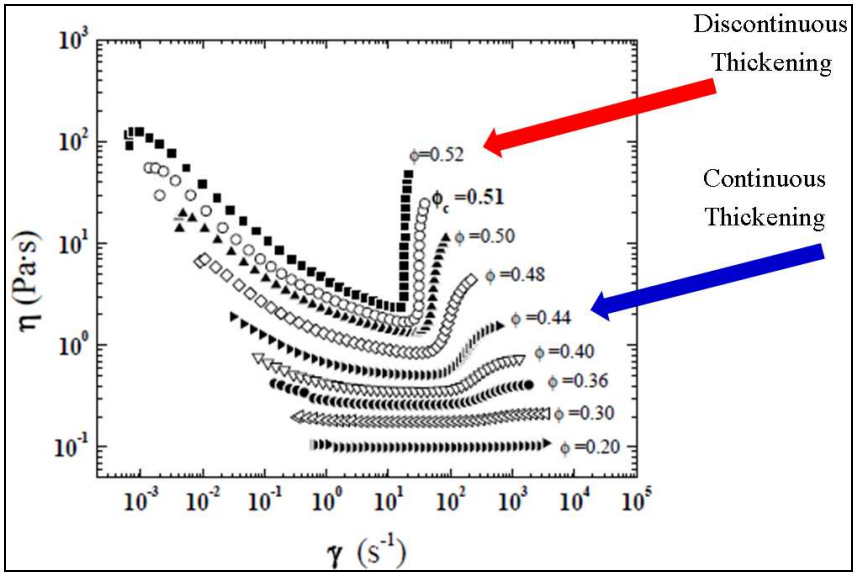

Figure 6: Continuous v. discontinuous shear thickening

Shear rates experienced by a protective garment can be approximated based on the thickness of the pad, and the speed of the impact. Given a shear rate, the particle loading needed to achieve a desired viscosity could be determined. For example, a garment with a thickness of 0.0254 meters (1 inch) undergoing an impact at 2 m/s would experience an initial shear rate of 78.7 s^{-1}. This corresponds approximately to the critical shear rate of an STF with a silica vol. % of 44, so any suspension with a higher particle loading will undergo shear thickening during the impact.

The rheology data shown above was obtained using a commercial rheometer (Rheometrics Scientific Corp. SR 5000) which involves placing a small fluid sample in a cell comprised of two disks. The lower disk is typically held static while the upper disk is rotated either in an oscillatory motion or at a continuous shear rate. A conceptual schematic of a rheometer is shown in Figure 7.

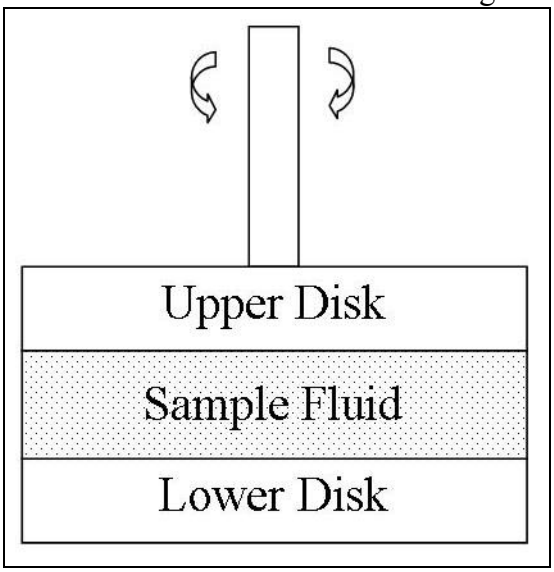

Figure 7: Conceptual schematic of a rheometer. Note: image not to scale

Unlike a radial shear of a rheometer, fluid movement during an impact will not likely involved shear in the radial direction as described above. In order to further discuss the behavior of a fluid in a protective garment, the type of flow must

first be established. The uni-axial compression of a protective garment or pad can be best approximated as squeeze flow.

1.4 Squeeze flow

In order to model the movement of fluid during an impact, the specific geometry must be defined. Because the floor and the body of the user will not significantly deform during an impact, one simplification is to assume they are flat plates. Fluid in the pad will be forced outwards as the pad is compressed during a fall. This type of flow is commonly referred to as squeeze flow.

Squeeze flow is a form of Poiseuille (pressure driven) flow in which a fluid plug initially sits between two plates. As one plate moves inwards, the fluid is squeezed from the inner gap. If the fluid obeys a no-slip boundary condition, the fluid will not flow out from between the plates initially, but rather will form a barrel like bulge at the edge leaving the contact area between the fluid and plates constant. Other possible boundary conditions include the fluid partially slipping from the plate with the rate dependent on compression rate, or perfect slip where the fluid flows freely across the plates [13]. Squeeze flow is further categorized by constant mass and constant area as seen in Figure 8 [13]. In the case of constant mass, the area of the plate is much larger than the initial contact area of the plug such that the full mass of fluid remains between the two plates during compression. In the constant area case, fluid is lost as the fluid undergoes radial flow leaving a smaller mass to be compressed beneath the same area. The fluid undergoing compression exerts a normal force on the top plate. This is analogous to the force transmitted to the femur. A more complete discussion of the forces will be in Chapter 3 which deals with simulation results.

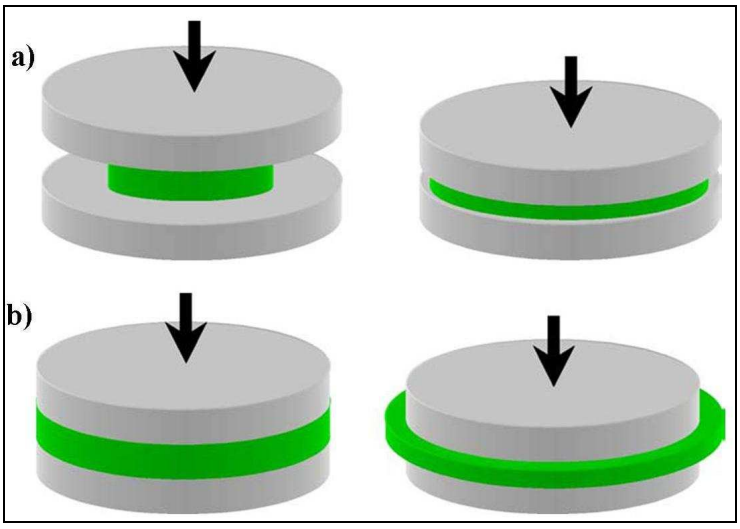

Figure 8: Squeeze flow under a) constant mass & b) constant area conditions

During an impact, the compression of the protective garment will account for only part of the overall response from the patient and garment. The layer of soft connective tissue, muscle and fat which surrounds the hip beneath the skin also provides nominal protection against impact. Moreover, the dynamics of a human fall are unique in that a fall consists of a variety of motions. If a person falls directly on their side, the motion is essentially pure rotational motion, though this is rarely the case. The modeling of bio-mechanics, and the mechanical properties of various human tissues, is an area of research that has grown significantly in the last decade or so as modern medicine seeks to gain a better understanding of the human body.

1.5 Previous biomechanical experiments regarding hip impacts

Dr. Stephen Robinovitch extensively researched the biomechanics of human falls and hip impacts [14]. During that time, he constructed a model for the prediction of forces on the femur through pelvic release experiments. The experiment attached patients to a pulley system while laying on their side with their legs and

shoulders supported. The pulley was released causing weight to be transferred to a force plate below the hip [15]. A schematic of his experimental setup can be seen in Figure 9; the inset image is the mechanical system used to model impact response during an impact [15].

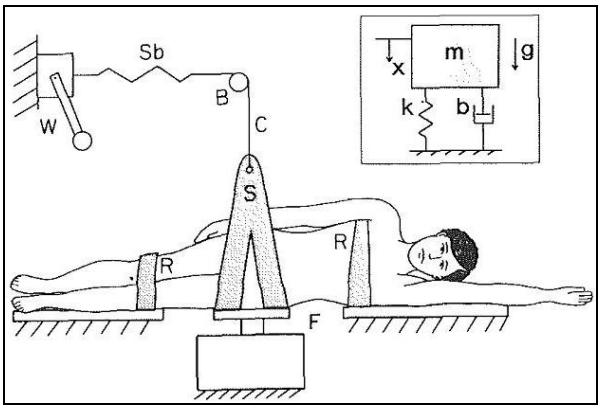

Figure 9: Robinovitch pelvic release experimental setup

From this mechanical model, Equation 1 was set-up as follows:

Equation 1: Mechanical model for femoral impact forces

$$m\left(\frac{d^2x}{dt^2}\right)+b\left(\frac{dx}{dt}\right)+kx=mg-F_N \tag{1}$$

From this setup, the normal force was the spring force, F_S, supporting the pelvis. By substituting the initial force divided by the spring constant, k, for the initial position, Robinovitch solved the model analytically to produce the form seen in Equation 2.

Equation 2: Femoral impact force, analytical solution

$$F=kx+b\left(\frac{dx}{dt}\right) \tag{2}$$

For female patients, the k and b values were 71,060 N/m and 561 N·s/m respectively for the relaxed muscle state. Muscles in state of higher activation (tense) were found to transmit greater force though the soft tissue to the bone [15].

Using his model, Robinovitch constructed predicted peak force curves for male and female patients in both relaxed and tense muscle states as a function of the drop height of the top of the hip. At a drop height of 0.7 meters, the predicted peak force for a female in the relaxed state was about 5 kN [15]. Using the relationship between potential and kinetic energy, the expected impact speeds would be 3.7 m/s. Identical models were developed in Matlab, creating the potential for modeling a human fall with a garment in place. In Robinovitch's work there were other key design metrics for later use with the inverted pendulum experiments. Assuming that the impact of the knee, shoulder, and hip were all roughly simultaneous, each impact would not affect the other impacts. Similarly, each of those three areas would be supporting a different effective mass. For female patients in the relaxed state, the effective mass supported by the hip was found to be 31 kg [15]. Using the impact speed discussed above, the total energy of the hip impact is 212.2 J. Finally, Robinovitch estimated that an unprotected hip will experience peak forces ranging from 5.6-8.6 kN [15]; the mean fracture force for an elderly hip is approximately 4.1 ± 1.6 kN [5]. This energy and maximum allowed peak force forms the basis for a successful protective garment used in this thesis.

There are many other researchers who have investigated the change in mechanical properties with age, gender, and other risk factors. Testing of cadaveric femurs from donors of varying age has shown that properties such as strength and stiffness can decrease by as much as 50% between a person's middle years (30s) and old age (60+) [16-18]. The tests also agree with many of Robinovitch's findings including female patients being at higher risk, as well as active muscle states resulting in greater peak forces than relaxed states [16-18]. Other predictions of mean fracture

force in the literature for a similar patient as described above show more variability. Roberts *et al.* found the force to be 2.8 ± 1.1 kN, Courtney *et al.* determined the force to be 3.4 ± 1.3 kN [19-20]. These forces are lower than those predicted by Robinovitch, possibly due to the use of cadaveric femurs.

1.6 Goal

The goal of this project is to better understand the behavior of a fluid impregnated foam composite for use in preventative medicine applications and other protective garments. Specifically, to meet the need for a lightweight flexible pad to prevent hip fractures in elderly patients. The pad needs to reduce the peak force of a 212 J impact to below 4.1 kN. If this can not be achieved, the fluid impregnated garment will need to outperform other commercially available garment. A model to aid in garment development will be generated alongside experimental work. A fluid will be selected based on its sensitivity, with respect to peak force, to changes in garment thickness and impact energy. Low sensitivity will suggest the fluid is robust despite changes in the impact energy for an individual patient. Finally, the amount of fluid used in making the garment will need to be minimized in order to keep the garment as lightweight, thin, and low cost as possible. The fluid will need to be dispersed in the pad such that the efficacy is not reduced by being worn vertically, and that the final garment is flexible so as to not cause patient discomfort.

Chapter 2

MATERIALS AND METHODS

2.1 Newtonian & shear thickening fluids

Because the thickening behavior of STFs varies strongly with particle type and volume fraction, experiments were performed to determine which fluid types might be the most appropriate for the application. In addition to STFs, various Newtonian oils were also tested to compare their protective performance.

The Newtonian fluids tested were polydimethylsiloxane (PDMS) oils with kinematic viscosities of 30,000 cSt (GE Viscasil 30,000) 100,000 cSt (GE Silicones 100M) and 500,000 cSt (Union Carbide Silicones L-45). Assuming a density of 960 kg/m^3, the oils had dynamic viscosities of 28.8, 96 and 480 Pa.s respectively.

The STFs used were 48 and 52 volume % Shokubai silica particles in M_W=200 PEG (Clariant), 45 vol. % Nanosil silica in PEG200, and 25 wt % Cab-o-sil TS-610 in M_W=1000 PPG (Bayer Arcol). Shokubai and Nanosil particles are both spherical silica with hydroxyl groups on the surface. Cab-o-sil particles are fumed silica particles that have been treated with dimethyldichlorosilane which replaces surface hydroxyl groups with methyl groups. These particles will typically form fractal agglomerates on the order of 0.2 to 0.3 microns in diameter. As seen in Figure 6, the 48 vol. % Shokubai mixture is continuously thickening, while the 52 vol. % mixture is discontinuous. The primary difference between the 52 vol. % Shokubai and 45 vol. % Nanosil is that the Nanosil particles have a higher polydispersity index

making them significantly less expensive. One important thing to mention about the 48 vol. % Shokubai suspension is that the particles will settle under gravity on a time scale of weeks, so mixing is required during storage. Rheology data for the STFs can be seen in Figure 10 [12, 21]. Data was not available for 25 wt. % Cabosil, 20 wt. % is shown instead for comparison. The STFs were prepared in batches ranging from 100-300 grams. A batch would be made by adding particles incrementally to the polymer solvent while hand mixing. Once the particles wet into the solvent, the batch would be allowed to sit on a roll mixer for at least 2 days before use.

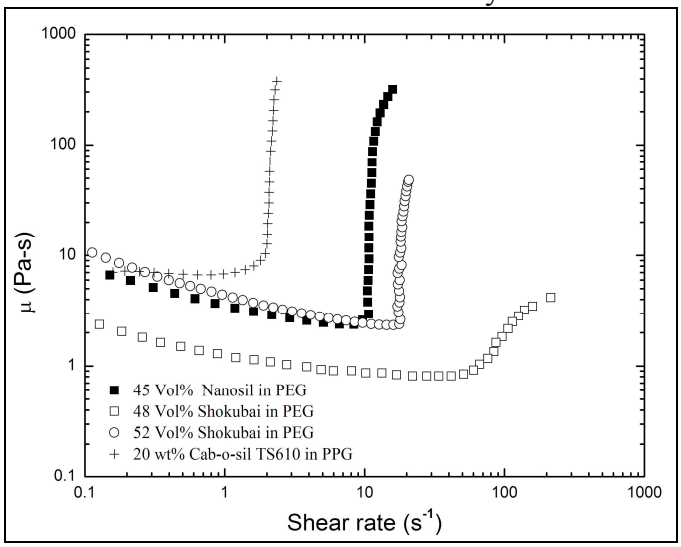

Figure 10: Rheology for STFs considered

In addition to fluid filled samples, closed cell ethyl vinyl acetate (EVA) foam (McMaster-Carr 86095K22 & 86095K24) was one of two materials impacted when adjusting the equipment before testing. EVA foam is typically soft, it is often used as a cushion in ski boots, as well as an insulator because it is waterproof, can withstand high heat, and is resistant to many chemicals. The other control material used was neoprene rubber mats (McMaster-Carr 9455K666) with varying stiffness. These mats when stacked together can approximate the mechanical properties of soft tissue. The spring constant of soft tissue as measured by Robinovitch was 71,000 N/m

[14]. The mats were layered with a 40 A mat and a 80 A mat in series for a thickness of ¼", or two 30 A mats, followed by a 40 A mat, and an 80 A mat totaling ½" in thickness.

In order to determine approximately how well the mats approximated soft tissue, the ½" layered mats were impacted. Previous work done by group members used these mats to achieve a peak force of 7.1 kN from a 25 J impact based on another source regarding the mechanical properties of soft tissue [22]. The impact shown in Figure 11 resulted in a peak force of about 8 kN. This increase in peak force is possibly due to the fact that the mats were not new when testing began. The spring constant was measured by fitting the initial linear region of the force v. displacement curve as seen in Figure 11.

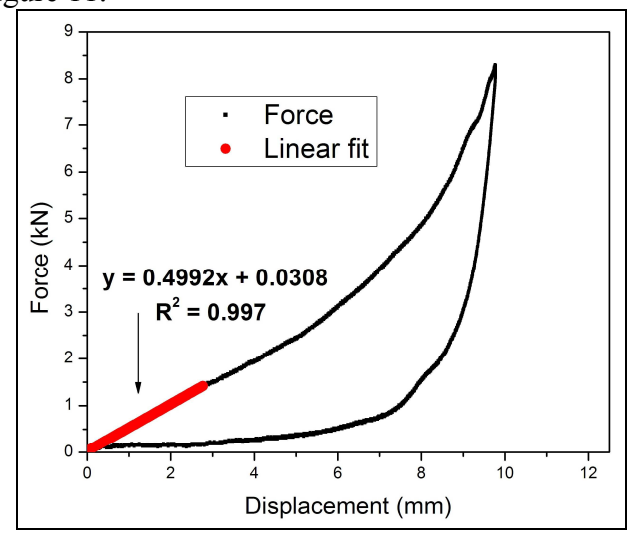

Figure 11: Force v. displacement for neoprene rubber mats impacted at 26 J

A total of five impacts were completed and analyzed producing an average spring constant of 499,680 ± 62,890 N/m. This is about an order of magnitude greater than the reported value. We continued using the mats based on the peak force match. It should be noted that the four mats were not bonded, unlike soft tissue, and had been used during impact tests before.

2.2 Sample preparation – single plug

Samples were made by containing a plug of the fluid in a sealed foam support. The support was made using EVA foam cut into 2" by 2 " squares. The center was then cut out using a round hole arch punch, commonly used for leather working, with a 1" diameter. The foam was then sealed to 4" by 4" squares of polyfilm (American Polyfilm, SO#2024) using a spray adhesive (3M 6065 Spray Mount) on one side. Test fluid was added by hand pouring, bubbles introduced through mixing were allowed to diffuse out for approximately one hour. The sample was then sealed using a second layer of polyfilm to cover the open surface, and the edges of the film were heat sealed to prevent fluid leaks after testing was complete. An unfilled sample can be seen in Figure 12.

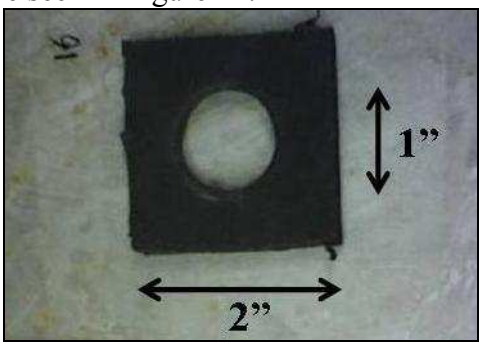

Figure 12: 1 inch plug drop tower sample

Fluid was added until the 1" diameter hole was filled completely. Samples were weighed before and after the addition of fluid. Variations in fluid weight were about 5%. Small air bubbles were typically present in samples, if large air bubbles persisted, samples would be allowed to settle longer before sealing. Final STF weights were 5-6 g for ¼" thick samples and 10-12 g for the ½" thick samples.

2.3 Sample preparation – area fraction

A single plug makes for poor garment design as the plug would need to be continuously centered over the greater trochanter to be effective, and would greatly

increase the weight. If the plug diameter was increased to ensure proper coverage, the STF would likely pool towards the base of the pad leaving the upper region exposed. One possible solution to this is to disperse the STF throughout the pad in multiple smaller pillars ($L/D \geq 1$) as opposed to a single, relatively shallow, pool ($L/D < 1$). Other group members have already carried out some impact testing at different area fractions (AF) by varying the spacing between pillars within the EVA foam support and impacting at 25 J [22].

The previous work was published in a confidential report, and the spacing of the pillars was controlled by laser cutting the foam. This preparation technique was not available, so samples were fabricated using hand tools. A 1" diameter round hole arch punch was used to make single plug samples (AF=1) as described above. A ⅜" Round Hole Arch Punch was used to make a 7-spotted honeycomb like pattern with each row spaced ⅓" apart and each column spaced ½" apart resulting in an area fraction of 0.33. Ideally the holes would be spaced closer together, but the punch had a tendency to drag the foam inwards while cutting. Two other area fraction were tested, also using a 7-spotted honeycomb pattern, but with holes equally spaced about 3 mm apart using cork borers (McMaster-Carr 6122A12), one with a 9 mm diameter (~.354") from a metric set (AF=0.50), and one with a ⅜" (~9.53 mm) diameter from an English set (AF=0.47). Area fractions were calculated for these samples by drawing a unit cell through the centers of the four pillars closest to the center pillar. This value differs slightly from the area fraction of STF beneath the impact head. The value reported is the relevant one when considering the cost and weight of the garment. Each of the four area fractions can be seen with a 1" impact head overlaid in Figure 13.

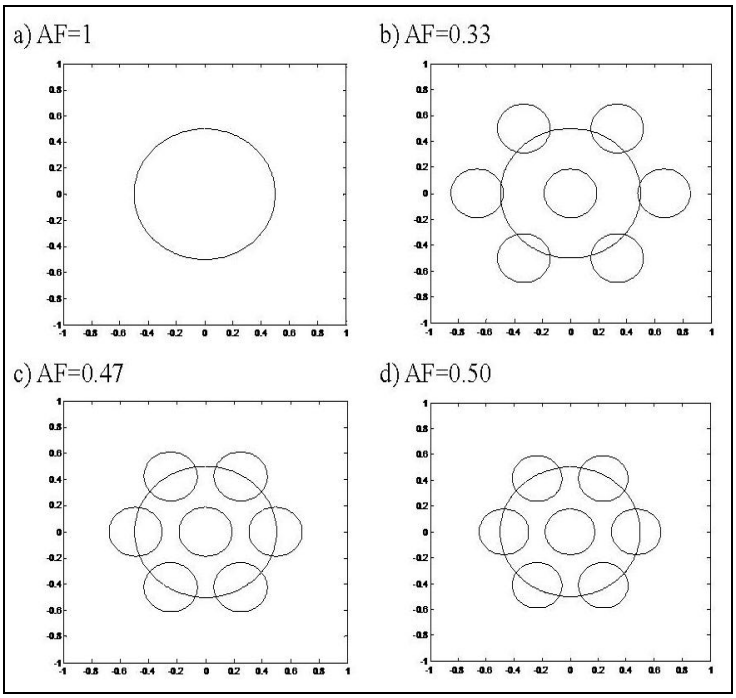

Figure 13: Area fraction targets.

For each of the area fractions tested, the diameter of the plugs are less than or equal to the diameter of the impact head. Final ¼" sample weights with the honeycomb pattern were typically about 1 g heavier than the single plug ¼" samples; ½" sample weight variation was < 2 g.

2.4 Experimental setup – drop tower

Impact experiments using linear motion were performed on an Instron 8200 drop tower, shown in Figure 14 [23]. The tower consists of a sample mount at the base, and a sled guided by two vertical rails. The sled has an interchangeable impact head, a load cell, and space for additional weight to be secured.

Figure 14: Instron 8200 drop tower

The impact head used was a 1" diameter flat ended cylinder. The sled and impact head, when used without additional weights, has a mass of 3.55 kg. Additional lead weights can be added bringing the total weight of the sled to 12.97 kg. The load cell installed on the tower had a max load rating of 9071.8 kg (20,000 lbs). The data acquisition software was set to collect for 50 ms after a photogate flag was triggered as the impact head reached the sample. Impact speed was controlled by adjusting the drop height and recording speeds as calculated by the data acquisition software. The software calculated displacement data from the measured impact speed and sled weight in addition to recording force.

2.5 Experimental setup – pendulum impact device

Though a drop tower experiment is capable of reaching the energies associated with a human fall, the motion of the impact is restricted to the z-axis. In order to properly test a prospective garment design, a system was needed that could produce the energy of a human fall, and the rotational motion associated with falling to one's side from an upright position.

To meet this need, an inverted pendulum impact machine designed by Richard Herseim in cooperation with the DuPont children's hospital was used [4]. The device consists of an aluminum frame with an aluminum arm 40" long attached near the base of the frame. The arm is equipped with several sensors. The first is a load cell 33.5" from the base of the arm nested inside a sample mount with a guiding piece for an impact head. Atop the arm, opposite the load cell, is a post for restrained added weights. There is a second load cell closer to the base of the arm such that an artificial femur can be mounted between the load cells hip the head of the femur in the first, and the knee at the second. An accelerometer is mounted at the end of the arm, and a potentiometer at the base. Data cables from each of the sensors plug into a National Instruments© (NI) data acquisition (DAQ) box which interfaces with a computer via USB. Key control panel components for the machine include an emergency shut off switch, a height adjustment switch which operates an electrical linear actuator, as well as a release lever powered by compressed air. Additionally, the frame has a second post for attaching counterweights at its rear. A picture of the machine loaded with an artificial femur and a foam 'garment' from Herseim's testing can be seen in Figure 15 [4].

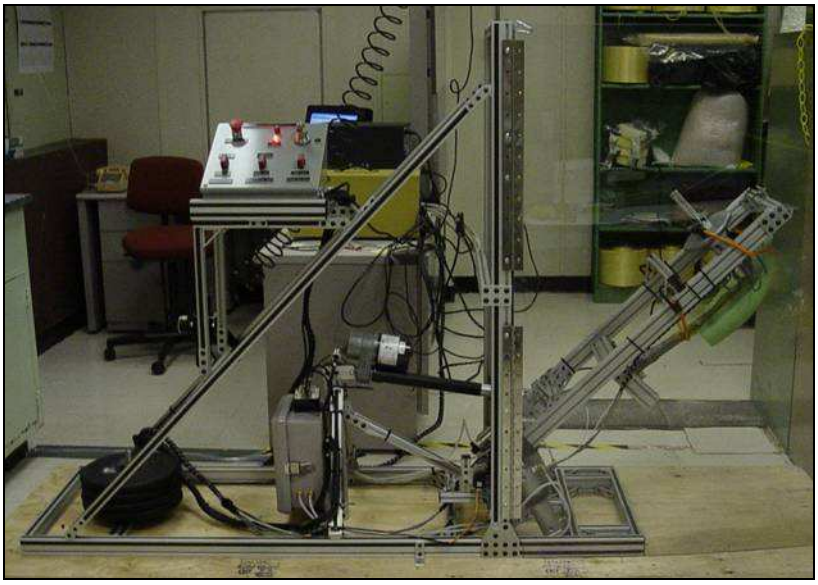

Figure 15: Inverted pendulum impact machine with sample loaded (left), counterweights (lower right), and instrument panel/DAQ box (top)

The impact head was similar to the drop tower impact head, with the contact area consisting of a 1" diameter flat cylinder as seen in Figure 16. The head was contacted to the load cell via a threaded bolt which could be screwed into the head to various depths to accommodate varied sample thickness.

Figure 16: Pendulum impact device impact head

In addition to load cells on the machine, testing at the University of Delaware Human Performance Lab involved the impact taking place over a force plate (AMTI) built into the floor capable of measuring the forces in the axial ('z') direction as well as in the lateral ('x' and 'y') directions giving us the possibility to quantify the rotational forces during an impact.

Data from the pendulum machine and force plates were received and processed by a NI Labview program written by a Dr. Stephan Thomas and Alan Needle, former and current PhD student of Dr. Charles Swanik. Recordable data includes position, speed (as calculated by differentiating position data, as well as by integrating acceleration data), acceleration, and the five forces described above.

Chapter 3

SIMULATIONS OF SQUEEZE FLOW OF NEWTONIAN FLUIDS & FOAM COMPRESSION DURING IMPACT

3.1 Introduction

Experimental data will ultimately determine the efficacy a garment. However, there are a number of other garment design considerations which may be simulated in order to save time and resources during experimentation. The simulation was built around squeeze flow of a Newtonian fluid. Various potential effects of the foam support were incorporated into later simulations. This arose from a need to determine the potential effects the foam support might have on impact samples, and how the mechanical properties of the foam can be manipulated to improve garment performance. Secondly, there was the question of whether the EVA foam would have a significant impact on the data acquired during impact testing. If so, a different support would be needed in order to isolate the effects of the fluid.

3.2 Matlab simulation of squeeze flow of Newtonian fluid

The normal force experienced by the moving plate during squeeze flow can be solved for using a full solution to the Navier-Stokes equation. The geometry as defined in Engmann *et al*. can be seen in Figure 17 in which H represents sample height and $\dot{H}$ represents the velocity of the top plate. The solution for a Newtonian fluid under no-slip conditions is a first order differential equation given in Equation 3

assuming fluid properties, and other experimental conditions, such as density and temperature remain constant throughout the impact [24].

Equation 3: Normal force from a Newtonian fluid, viscous contributions only

$$F_N = -\frac{3\pi \mu R^4 \dot{H}}{2H^3} \tag{3}$$

When the normal force is re-written in terms of acceleration according to Newton's second law of motion ($F=ma$), the result is a second order differential equation which can be solved as part of a series of differential equations in Matlab. The derivation for this series of differential equations can be seen in Appendix A. The code used is in Appendix B.

While Equation 3 accounts for viscous resistance, it does not account for the inertia of the fluid being displaced. A similar form of Equation 3 combines the viscous contributions with the inertial contributions resulting in Equation 4 [25].

Equation 4: Normal force from a Newtonian fluid, viscous & inertial contributions

$$F_N = -\frac{\pi R^4}{4}\left(\frac{6\mu \dot{H}}{H^3} + \frac{3\rho \ddot{H}}{5H} - \frac{15\rho \dot{H}^2}{14H^2}\right) \tag{4}$$

Equation 4 will simplify to Equation 3 when inertia is negligible. Both of these equations were solved using the ode45 differential equation solver in Matlab to produce acceleration, speed, position/displacement, and force data for a simulated impact. The speed and mass of the top plate matched the experimental conditions of the drop tower experiments discussed in Chapter 2. A comparison of the two simulation results can be found in Figure 18 for the 1 m/s impact speed on the 28.8 Pa.s oil where inertial effects were the most substantial relative to viscous effects. This can be shown using the dimensionless Reynolds number, defined as the ratio of inertial to viscous forces, shown in Equation 5.

Equation 5: Reynolds number

$$R_e = \frac{\rho V D}{\mu} \tag{5}$$

The density of PDMS oil is approximately 965 kg/ m^3. V is the velocity of the fluid, and D is the diameter of the flow field. In this case, using the initial speed and plug diameter, a Reynolds number of 0.85 is obtained. 28.8 Pa-s was the lowest viscosity to be tested, so viscous forces will be even more dominant for other samples. The same impact for the 96 and 480 Pa-s oils would produce Reynolds numbers of 0.25 and 0.05 respectively.

Reynolds number will increase linearly with speed meaning that at higher energies inertial effects will be greater. However, because of the resistance to flow seen in STFs, velocities will be high initially, and decrease rapidly throughout the impact.

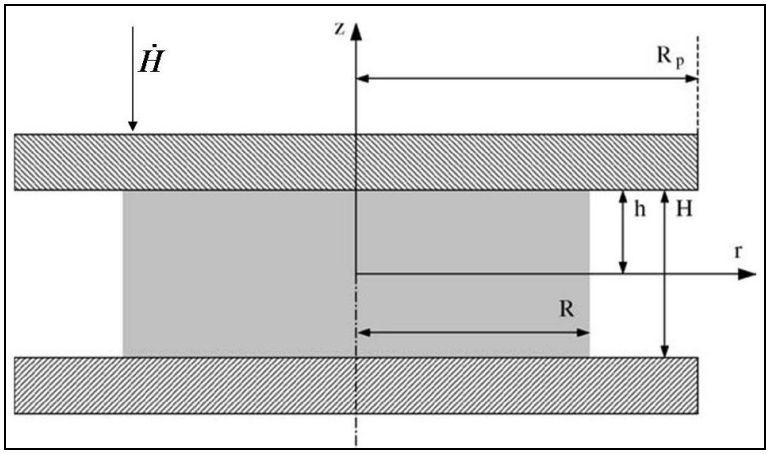

Figure 17: Squeeze flow geometry

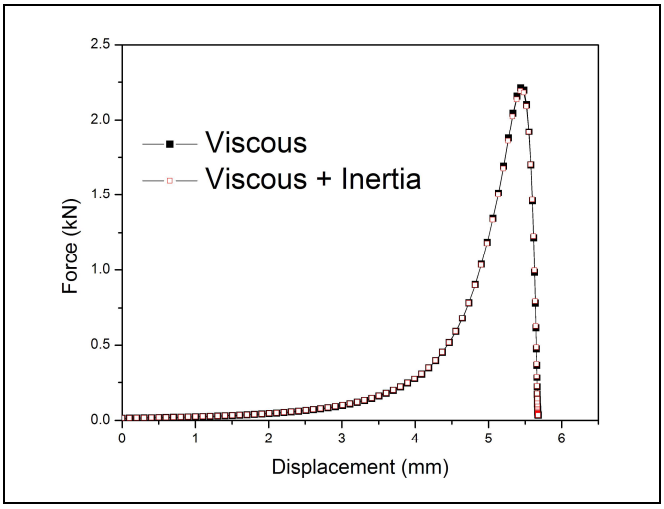

Figure 18: Comparison of viscous only and viscous + inertia simulations

Because overcoming the inertia of the sample's mass dissipates additional energy, the peak force predicted by the later model is slightly lower. However, because the mass is small relative to the energy input, predicted peak forces varied by about 1.5% and the inertia terms were dropped in subsequent calculations. By using the viscous effects only, the complexity of the simulation was minimized.

Simulations matching the experimental conditions for the Newtonian oils were run. The experiments will be described in more detail in the following chapter. The model predicted decreasing peak force with increasing viscosity, as well as a decrease in total displacement as seen in Figure 19. Lower viscosity oils take longer to reach their peak forces, shown in Figure 20, indicating that the oil has been displaced further for the same amount of energy dissipated. As the oil is displaced further, the shape of the curve around the peak force becomes narrower. The limit of this behavior would be an impact between two plates with no fluid, in which case the slope of the force v. time curve would be nearly infinite. The experimental date does show the predicted decreasing trend in peak forces with increasing viscosity.

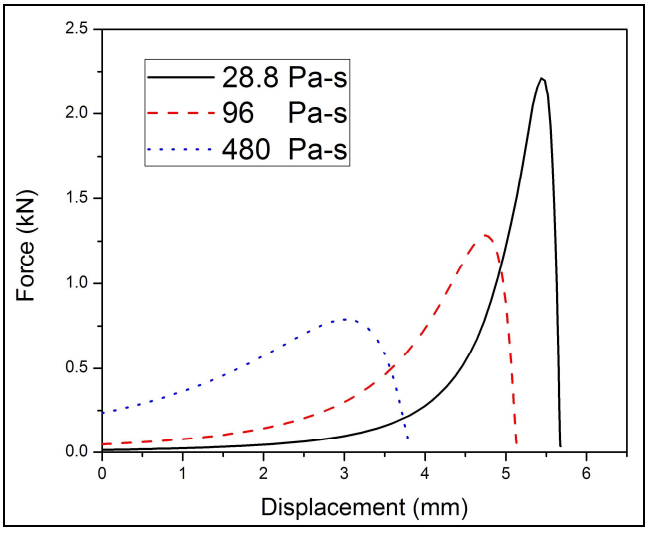

Figure 19: Force v. displacement - 1 m/s simulated impact of 1/4" thick plug of Newtonian oil

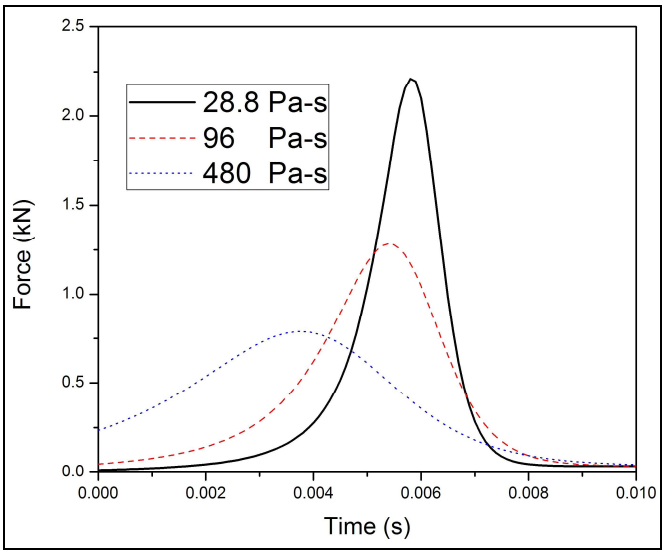

Figure 20: Force v. time - 1 m/s simulated impact of 1/4" thick plug of Newtonian oil

Figure 21 shows a comparison of the peak forces as observed experimentally and predicted in the simulation, as well as the greatest success in predicting curve shape. For the other viscosities tested, curve shape was similar, though displacement values did not agree as closely.

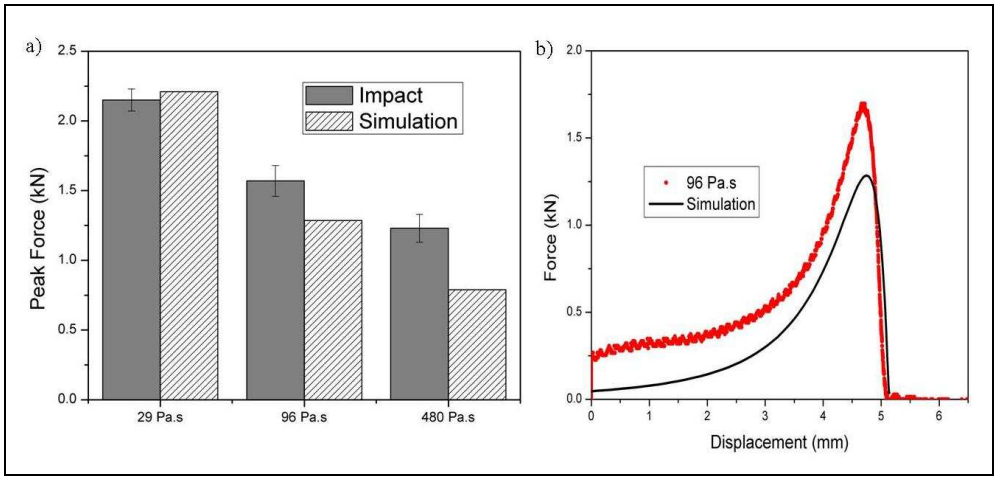

Figure 21: a) Peak force comparison for 1/4" samples at 1 m/s.
b) Force v. displacement comparison from same sample set

3.3 Matlab simulation of squeeze flow of a power law fluid

Having established the Newtonian simulation as effective for the purposes of trend prediction, a simulation of STF squeeze flow was achieved by modeling an STF above and below the critical shear rate as a piece-wise power law fluid. The normal force for a power law fluid is given by Equation 6 where viscosity is defined by the pre-exponential and exponential factors K and n from Equation 7 [26].

Equation 6: Normal force from a power lab fluid, viscous contributions only

$$F_N = -\frac{2\pi\left(2+1/n\right)^n}{n+3} K\dot{H}\left|\dot{H}\right|^{n-1} H^{-(2n+1)} R^{n+3} \tag{7}$$

Equation 7: Viscosity of power law fluid

$$\mu = K\dot{\gamma}^{n-1} \tag{8}$$

Fitting K and n values to experimental rheology data proved to be a very sensitive operation when attempted. The ability of differential equation solvers in Matlab to handle the rapid changes in viscosity upon initial contact was insufficient. Results produced by Matlab typically involved either non-real answers, or

instantaneous spikes in peak force upon first contact that were orders of magnitude above what would be expected.

For demonstration purposes, K and n values of 0.5 and 2 were selected to show potential behavior for a shear thickening fluid above its critical shear rate. The simulation was run under the same conditions as the Newtonian fluid simulation. The result is shown in Figure 22.

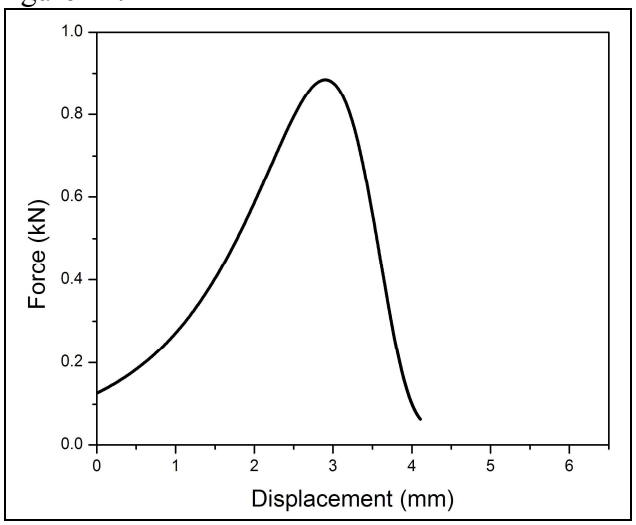

Figure 22: Force v. displacement of a power law fluid impacted at 1.78 J

This result demonstrated the potential usefulness of the power law model to garment design. However, a complete predictive model can not be developed until the problems with non-linear curve fitting are resolved such that the model can simulate fluids with known properties.

3.4 Foam compression simulation

Fluid plugs dispersed in a real garment would not be the only source of protection during an impact. The foam support for the fluid plug would also be compressed in the axial direction, as well as in the radial direction, as the fluid plug expands. Assuming the foam is sufficiently soft, it will have little effect on the

performance of the pad. Several simulations were developed in order to test this. The first involved treating the foam as a linear Hookean spring surrounding the plug. During an impact, the contact area between the plate and the plug is kept constant as dictated by the size of the impact head. As the plug expands radially, it's motion is resisted by the foam exerting a force acting against the flow of the plug, slowing the rate of axial compression and exerting a greater normal force on the top plate. The derivation for the foam spring model can be seen in Appendix C. The spring model was tested varying the Young's modulus (*E*) by orders of magnitude from 0.01 MPa to 10 MPa with the original simulation result as a control. The simulation results can be seen in Figure 23 for the 28.8 Pa-s Newtonian oil in a ¼" plug impacted at 1.78 J (1 m/s, 3.55 kg). As a reference point, the Young's modulus of a couch cushion is about 0.01 MPa [27].

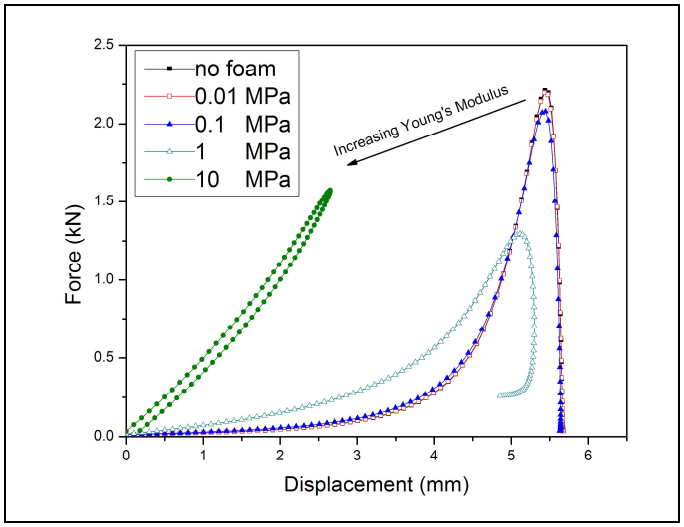

Figure 23: Simulation of the effect of Hookean foam support

The Hookean spring simulation was run for the other oil viscosities tested on the drop tower. Their predictions were similar to those found in Figure 23. The effect of the foam is negligible for E < 1 MPa. The trend in peak forces is two fold.

Initially, peak force is reduced as E increases as the plug is held in place longer and dissipates more energy as it flows. Above a critical E, the strength of the foam outweighs the previously mentioned benefit and the peak force begins to rise with increased modulus, rather than fall. For the 96 Pa-s oil, the critical modulus was in the same region as the 28.8 Pa-s oil, or between E=1 MPa and E=10 MPa. For the 480 Pa-s oil, the critical modulus lay between E=0.1 MPa and E=1 MPa. Foams with a Young's modulus of less than 1 MPa had no significant effect on peak force, regardless of the fluid.

Several other models were tested to confirm this. One placed a theoretical foam spring in parallel with the fluid plug so there were no interactions. The area of the foam spring was varied from 10% to over 100% of the area of the plug. In another model, the impact head was changed to a flat plate covering the entire foam and fluid sample described in Chapter 2.1, and both the fluid and foam were compressed axially while the fluid and foam resisted each others' expansion in the radial direction. The effect of the foam remained negligible below E= 1 MPa in the case of the foam spring as shown in Figure 24a. However, in the case of the plate, the effect of the foam was visible at E= 0.01 MPa. Below E= 1 MPa, the effect of the foam is about a 25% reduction in peak force for the lowest viscosity oil at the lowest impact energy tested seen in Figure 24b.

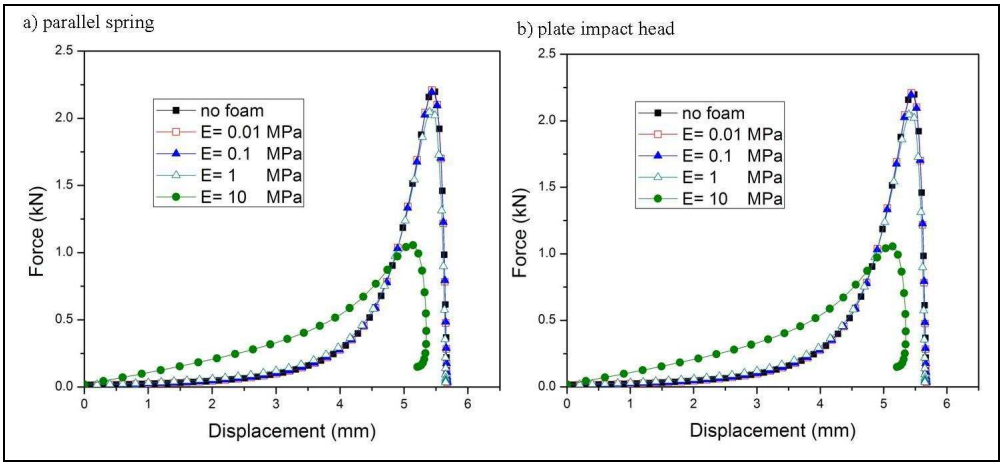

Figure 24: Simulated impact of 28.8 Pa-s Newtonian oil with 1.78 J with a) foam spring & fluid in parallel and b) plate impact head

Knowing that a real impact will not involve a rigid plate like the one simulated, the results of the plate impact simulation only further confirms the need for the foam used to have a Young's modulus below 1 MPa for fluid testing as suggested by other simulations. In addition to predicting the modulus needed for the isolation of fluid in performance testing, the models are now capable of making predictions regarding the performance of a fluid/foam composite garment. The simulations predict that garment performance can be improved by using a foam with a higher Young's modulus up to 10 MPa.

3.5 Mechanical testing of EVA

In order to determine if the EVA foam used during the drop tower experiments was having a significant effect on the performance on the sample, sections of EVA foam were compressed in an Instron Mini 44 to strains of about 90% using a maximum load of 1 kN. The foam was allowed to sit on a flat bed while compressed by a 1" diameter flat impact head. The Young's moduli can be seen in Table 1. The near linear region, and linear fit, for the ¼" EVA foam is the inset image in Figure 25 below.

Table 1: Young's modulus for EVA foam

Foam	Young's Modulus (kPa)
¼" EVA	4.51
½" EVA	3.75

The measured Young's modulus for both samples was <0.01 MPa, so their effects at low strains would likely be negligible. However, the strain range over which these values were measured was 0 - 10%. In a real garment, the total strain would likely be well above 50%. At high strains, the stress-strain relationship was highly non-linear.

The stress-strain data was therefore fitted to a third order polynomial, Figure 25, and the resulting polynomial was added to the plate impact model in which both the foam and fluid are axially compressed. The simulation results for the polynomial fit for EVA and the Hookean spring can be seen for the ¼" sample filled with 28.8 Pa-s oil impacted with 1.78 J is in Figure 26.

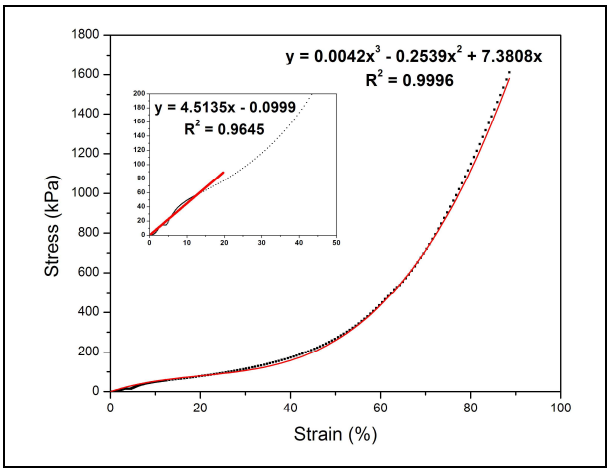

Figure 25: Engineering stress-strain data for 1/4" EVA foam

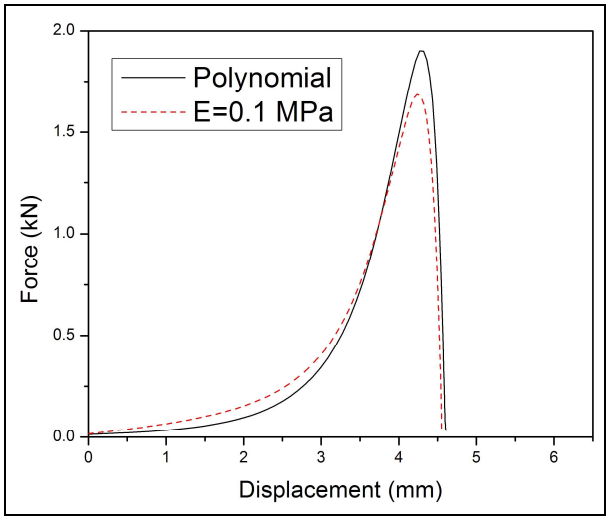

Figure 26: Simulated impact results for polynomial fit EVA and 0.1 MPa foam

Although the effects of the "polynomial fit" foam are visually more noticeable on force v. displacement plots than the Hookean foam, the relative increase in peak force is slight. Furthermore, the total displacement remained about the same showing that neither foam is significantly inhibiting the radial expansion of the fluid in the sample. When the Newtonian oil is replaced by a discontinuously thickening STF, the displacement will be smaller further reducing the possible contributions of the foam at larger strains.

3.6 Simulation conclusions

Simulations of squeeze flow have shown that even at energies well below that of a human fall, the inertial contribution to energy dissipation are insignificant relative to viscous dissipation. Although inertial effects will increase with energy, the relative effects should still be insignificant because of how rapidly velocity decreases during an impact. By simulating foams with a range on mechanical properties, it has been shown that material with a Young's modulus of less than 1 MPa will not have significant contributions to fluid performance. Furthermore, the effect of stiffer foams

on pad performance varies, first improving then decreasing performance by their resistance to axial compression, or by restricting viscous dissipation of energy through radial expansion of a fluid plug. Foam with a Young's modulus below 10 MPa improved performance in all simulations. The EVA foam currently in use will likely remain a good candidate for garment design as testing moves to higher energies.

Chapter 4

CHARACTERIZATION OF NEWTONIAN AND NON-NEWTONIAN FLUIDS FOR POTENTIAL PROTECTIVE GARMENT APPLICATIONS

4.1 Introduction

The peak force design metric is centered around an elderly female patient in a muscle relaxed state. Based on the peak force predictions from Robinovitch, the peak force experienced by this patient is the lowest of the other three scenarios he discussed. In order to ensure the garment is robust for a variety of patients, selection of the fluid is key. The performance of the fluid should have as little sensitivity as possible to changes in sample thickness and impact energy. Low sensitivity to thickness gives a greater increase in performance for increases in thickness, helping to minimize the final thickness of the garment. Low sensitivity to changes in energy provides similar returns when trying to protect against patients of varying height, weight, etc.

4.2 Experimental set-up

The samples tested in this chapter include all fluids describes in the materials section including both Newtonian and shear thickening fluids. The sample geometry used was the 1" diameter single plug in EVA foam.

Each type of fluid was tested at sample thicknesses of ¼" and ½". The purpose was to gain insight into the effect on performance, regardless of fluid type, with regard to peak force for varying sample thickness. It is possible that the peak

force sensitivity to thickness changes will vary for different types of fluid. Ultimately, the garment should be as thin as possible, to limit patient mobility issues and cost, while achieving the desired protection.

Each sample type was also tested at two different energies, 1.78 J & 7.10 J; corresponding to impacts at 1 and 2 m/s using the minimum weight (3.55 kg) on the drop tower. This test will be useful for predicting which fluids are most sensitive to changes in impact energy. The tests are at energies two orders of magnitude below that of a human fall, so low sensitivity would be a desirable quality. This difference in energy is too great for a simple extrapolation, but the low test energy may help resolve differences between the sample types. Before each experiment, the photogate flag height was adjusted to the proper height depending on sample thickness, and the drop height was varied until the desired speed was reached.

For every thickness, energy, and fluid type, three samples were fabricated and impacted. In cases where a single curve is shown, it is a representative sample from the set of three. Error bars shown are standard deviations calculated from the three samples. The matrix of samples completed is shown in Table 2. Sample weights and peak forces for these experiments can be found in Appendix D.

Table 2: Sample matrix for fluid selection experiments

Thickness (inch)	**1/4"**	**1/4"**	**1/2"**	**1/2"**
Energy (J)	**1.78**	**7.1**	**1.78**	**7.1**
28.8 Pa.s	x		x	x
96 Pa.s	x		x	x
480 Pa.s	x		x	x
25 wt.% Cabosil	x	x	x	x
48 vol.% Shokubai	x	x	x	x
52 vol.% Shokubai	x	x	x	x
45 vol.% Nanosil	x	x		

4.3 Performance comparison of fluid to foam

Because of the weak mechanical properties of EVA, impacts on both the Newtonian oil and STF samples resulted in peak forces lower than unfilled foam by about a factor of 2, as seen in Figure 27. This force v. displacement plot shows the foam reaching a maximum strain of about 50%, whereas the STF displaces about 75%, and the Newtonian fluid displaces almost entirely during the impact.

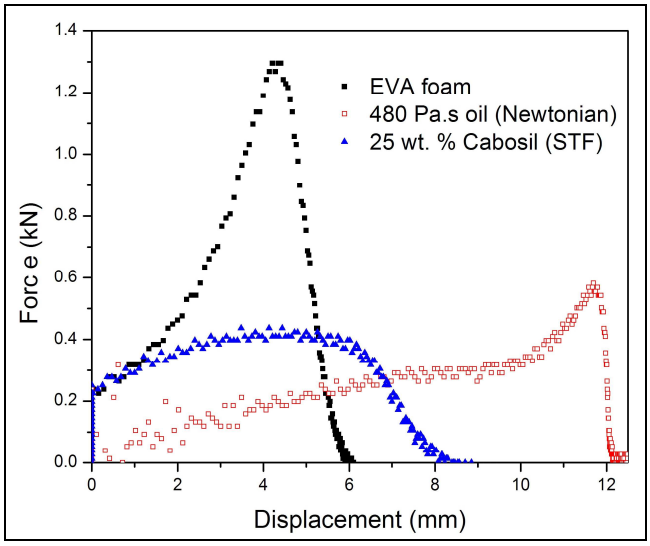

Figure 27: Comparison of foam and fluid ½" thick samples at 1.78 J

The factor of two reduction in peak force in both of the fluid samples over the EVA foam is encouraging. Although the type of foam used in a protective garment would likely have a higher Young's modulus, the performance of that foam would also likely depend strongly on the number of times it has sustained an impact. The EVA sample shown in Figure 27 had an imprint of the impact head left afterwards, and did not return to its original thickness of ½". Once the issue of containing the fluid is addressed, the fluid filled pad has the potential to perform better over the course of repeated impacts. The seal between the foam and polyfilm was intended to be weak so

that the influence of the fluid on normal force could be isolated from possible effects of the foam.

This comparison revealed a significant limitation of the drop tower and its included software. In theory, the energy absorbed by the pad should be equal to the initial kinetic energy. The only continuous sensor on the drop tower is the load cell, and the only information given to the software is the mass of the sled and the impact speed taken from the photogate. Force data is converted using mass to acceleration. Displacement is then calculated using acceleration data and the initial velocity. The Riemann sum of force versus displacement data gives the total energy absorbed. The energies for the three samples seen in Figure 27 is shown in Figure 27.

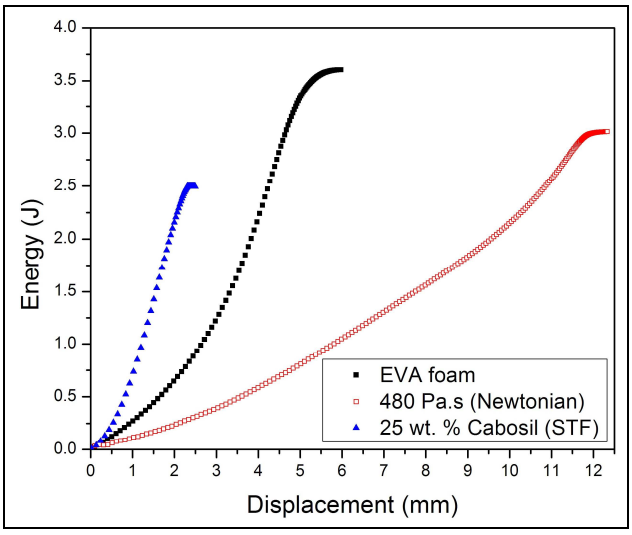

Figure 28: Absorbed energy of ½" thick samples of foam and fluid at 1.78 J

The absorbed energies all exceed the predicted 1.78 J, and by varying amounts. The same values are obtained when the Riemann sum is performed manually from the force and displacement data. The error in the calculation is in the accuracy of the conversion of the force data, and the ensuing double integration. Proper placement of the photogate flag also contributes when comparing samples taken at different times.

This is supported by the observation that within a set of samples, the calculated energies have nearly the same error resulting from the same impact speed and photogate flag placement.

4.4 Effect of viscosity of Newtonian oil performance

In the case of the Newtonian oils, higher viscosity resulted in better performance as predicted by the model. However, samples filled with Newtonian fluids tended to squeeze nearly flat, which is reflected in the peak displacement values in Figure 29. Figure 29 also shows the benefit of increased pad thickness as each ½" Newtonian oil sample outperforms its ¼" counterpart by approximately a factor of 2. Significant performance gains were expected, especially with Newtonian fluids where the force is proportional to the inverse of height cubed, see Equation 3.

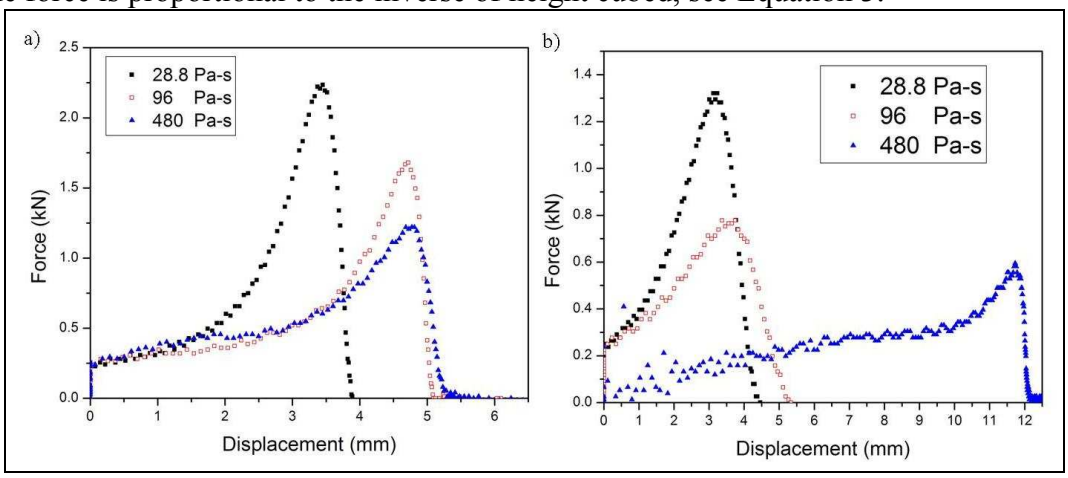

Figure 29: Newtonian oil force v. displacement curves for a) 1/4" and b) 1/2" samples at 1 m/s

It is immediately apparent that if a Newtonian fluid were to be used in a protective garment that the viscosity would need to be significantly higher than those tested here. If a garment containing a Newtonian fluid were used and the fluid needed to displace entirely in order to provide sufficient protection, the garment would need to be single use or be very well sealed. All samples containing Newtonian fluids were

squeezed nearly flat during testing though this is not reflected by the final displacement values predicted by the drop tower software. Although foam garments do not currently provide adequate protection, they have the advantage of being easier to reuse. STF samples impacted were more resistant to squeezing out of their plugs than the Newtonian oils because of their higher viscosities under shear.

4.5 Effects of sample thickness

As discussed above, the effect of sample thickness needs to be determined in order to determine the performance of a garment of a given thickness. Patient compliance is low regardless of garment thickness [8-9]. As a result, this project did not define a maximum thickness constraining the garment. It is still imperative to make the garment as thin as possible for issues of patient comfort and mobility as well as garment cost. This assumes that compliance will increase with decreasing garment thickness.

A summary of the samples with regard to changing sample thickness can be seen in Figure 30. The 480 Pa-s oil results were shown for comparison; the same sample set at 2 m/s included the impact head bouncing and re-impacting on the crushed sample resulting in a peak force higher than the initial impact.

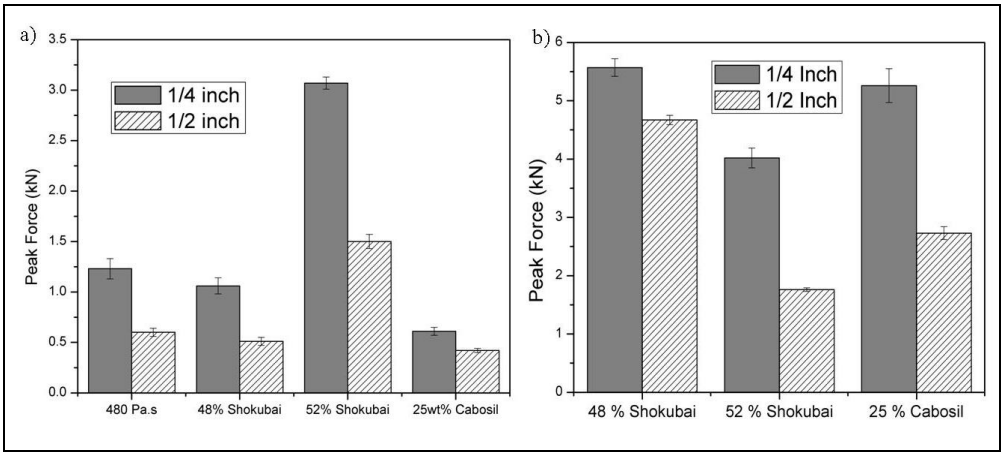

Figure 30: Effect of sample height comparison for a) 1 m/s and b) 2 m/s

At low energies, the benefit of a thicker sample is not immediately clear as improvements in performance vary strongly with sample type. The vast majority of samples exceeded the 4.1 kN allowed, though this test was done by striking the pad directly with the impact head without soft tissue which attenuates the force. In the case of the 52 vol. % Shokubai samples, the STF thickens almost instantaneously, giving it the poorest performance at low speeds and a 50% cut in peak force with the doubled sample thickness. The other STFs outperformed the 480 Pa-s oil at 1 m/s, and all STFs outperformed at 2 m/s. This suggests that STFs will outperform Newtonian fluids at higher energy, and selection will be a question of thickening response.

The 48 vol. % Shokubai, and to a lesser extent the 25 wt. % Cabosil, were unique in that performances was effected less by the sample thickness. Their failure to protect at higher speeds is the result of their ability to flow during the impact. Unlike the 52 vol. % Shokubai samples, the continuously thickening samples appeared similar to the Newtonian samples in that the final displacement of the fluid is close to the original sample thickness. This trend in displacements is shown in Figure 31.

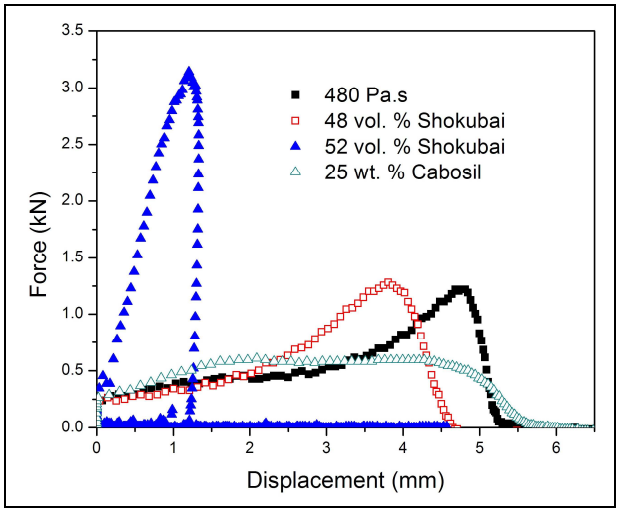

Figure 31: Force v. displacement of 1/4" thick fluid samples with 1.78 J

4.6 Effect of impact speed

Just as the effect of pad thickness is an important metric in producing a garment with the aesthetics and comfort requirement of an elderly patient, so too is the effect of impact speed on garment performance. The design metrics listed above refereed to a patient with a specific weight, bone strength, etc. The final garment must be able to protect patients that a differ from the weight and height used in determining the design metric. Figure 32 shows a comparison of samples of the same height impacted at both 1 and 2 m/s. The samples are the same shown in Figure 30, they are reorganized here to show speed differences side by side. Keeping in mind that the difference between these two impacts in a four fold increase in Energy, the performance variation is crucial to selection of an STF for testing at higher energies like that of a human fall.

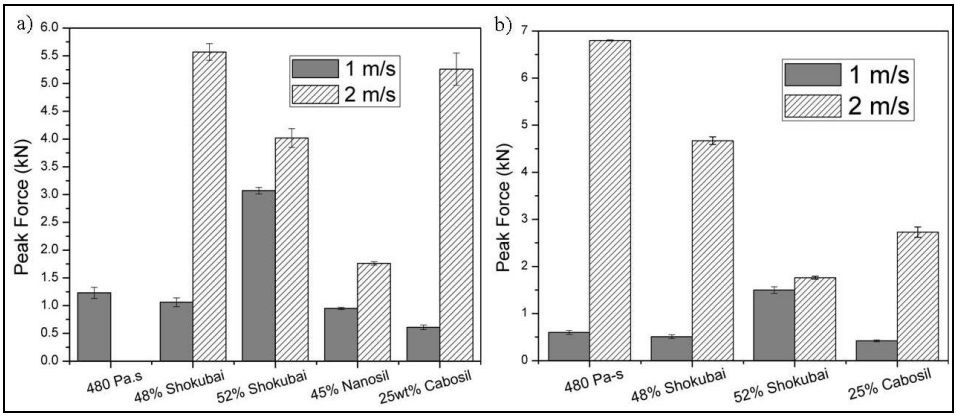

Figure 32: Effect of sample height comparison for a) 1/4" and b) 1/2" thick samples

The need for the fluid to be capable of performing well at higher speeds is critical as changes in speed produce much greater changes in total energy. Here, both the 48 vol. % Shokubai and 25 wt. % Cabosil samples allow peak forces more than four times greater when energy is quadrupled. By comparison, the 52 vol. % Shokubai and 45 vol. % Nanosil both allow peak force increases of less than 100%. In the case of the ½" samples, the peak force increases by a nearly insignificant 10%. The 45 vol. % Nanosil suspension was selected as the fluid of choice over the 52 vol. % Shokubai because Nanosil particles cost about $6.5 per kg, and Shokubai particles cost about $800 per kg. About 60% of the STF weight of each sample is particles, so this cost difference is quite significant.

4.7 Fluid Selection Conclusions

Newtonian fluids are poor performers, even at relatively low energy impacts. In the cases where they are effective relative to a STF, they have the greatest total displacements as seen by the sample condition after impact, as well from the shape of the force v. displacement curve. Continuous STF suspensions performed well with little variation in allowed peak force with respect to the thickness of the sample. However, performance did not scale linearly with increased energy and

samples had the same displacement tendencies as the Newtonian oils. This coupled with the tendency for the 48 vol. % Shokubai particles to settle makes them a poor choice for a garment intended to last years.

Finally, the discontinuous STFs had performed poorly at the lowest tested energies. Because these mixtures thicken quickly, more force is transmitted through the pad during the impact. However, the performance of these mixtures is the least sensitive to changes in impact speed which makes them a good choice for testing at higher energy. Because of the strength of their thickening responses, they have the smallest displacements making them good candidates for a reusable garment. Continuing on the product viability case, the 45 vol. % Nanosil mixtures was selected for further testing over the 52 vol. % Shokubai given the cost of the particles.

Chapter 5

EFFECT OF AREA FRACTION OF STF ON PAD PERFORMANCE

5.1 Introduction

As discussed in Chapter 1, there are a number of design metrics in addition to peak force which must be considered in garment design. Among them are the weight, flexibility, and cost of the pad. The STF is by far the heaviest and most expensive material, so limiting its use is crucial. One way to do this is to decrease the area fraction of fluid used by dispersing the STF in smaller pillars across the pad rather than filling the entire pad with fluid. By separating the pillars with soft foam, the garment will maintain its flexibility while being worn.

5.2 Experimental setup

Samples were fabricated for all four area fractions shown in Figure 13 for testing on the drop tower. On the pendulum impact device, samples with area fraction of 0.47 and 1.00 were used. In all cases, the STF used was the 45 vol.% Nanosil particles in PEG200 as selected in Chapter 4. The STF was carried by the same ¼" and ½" EVA foam. For each of the sample types, three were made and tested. Because the energy was carried out at higher energies, the neoprene rubber mats were used as a control.

In order to attain the desired impact speed, the neoprene mats were placed below the impact head ordered with the stiffest facing the impact head. This is to

compare the performance of the un-aided STF pads to the body's soft tissue. During testing on the drop tower, samples were positioned at the base such that the falling impact head would strike as close as possible to the center of the target striking all STF pillars. On the pendulum impact device, samples were attached to the impact head using double sided tape to ensure the sample was centered properly.

On the drop tower, additional lead weights were added bringing the total weight of the sled to 12.97 kg. Impacting at a speed on 2 m/s produced an impact energy of 26 J. The impact head was the same 1" diameter flat cylinder used in previous experiments.

On the pendulum impact device, 25 lbs (11.34 kg) were added to the arm. The arm was raised to give the hip region of the arm an impact speed of 2.1 m/s (drop height ~13.5"). Total impact energy was 25 J. The impact head was custom built by the chemical engineering department machine shop with an adjustable shaft so that samples would be impacted flat against the ground regardless of thickness. The contact area of the head remained a 1" diameter flat disk like the drop tower impact head.

The matrix of samples tested can be found in Table 3. Sample weights and peak forces for all drop tower and pendulum impactor experiments can be found in Appendix E.

Table 3: Sample matrix for 45 vol. % Nanosil targets for area fraction experiments

Drop Tower	**26 J**			
Area Fraction	0.33	0.47	0.50	1.00
Thickness: 1/4"	x	x	x	x
Thickness: 1/2"	x	x	x	x
Pendulum Impactor	**25 J**			
Area Fraction	0.47		1.00	
Thickness: 1/4"	x		x	
Thickness: 1/2"	x		x	

5.3 Drop tower results

Figure 33 shows the results of the area fraction testing on the drop tower. Similar to the previous drop tower experiments, the doubling of sample thickness decreased peak force significantly, here by 50-70% depending on area fraction. As expected, higher area fraction samples performed better given the larger amount of STF beneath the impact head.

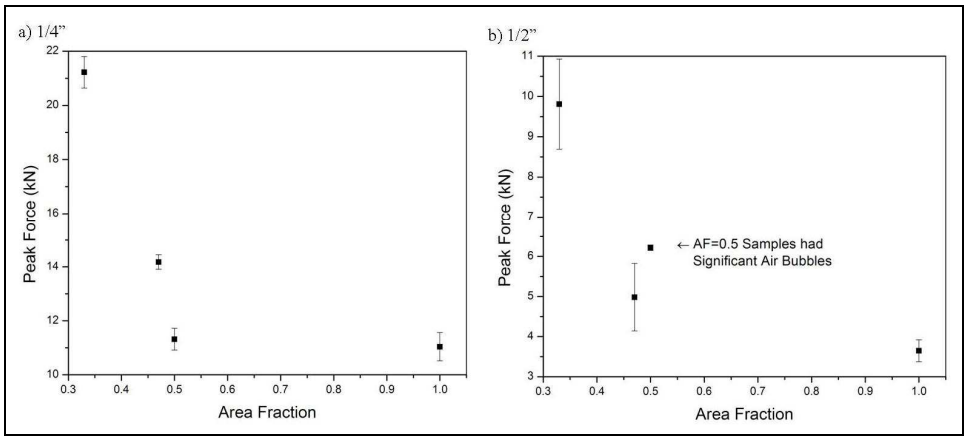

Figure 33: 26J impact results for a) 1/4" and b) 1/2" samples

Interestingly, the marginal benefit to increased area fraction appeared to diminish above about AF=0.50. The single plug (AF=1) samples outperform the AF=0.50 samples by about less than 10% for the ¼" case, and outperform the AF=0.47 samples by 20% in the ½" case. More experiments would be needed to better determine the location at which the benefit of increased area fraction diminishes beyond the need to make the garment lightweight, low cost and flexible. Further testing would also help determine if this critical area fraction is independent of sample thickness.

5.4 Pendulum impact device results

Figure 34 shows the results of the impacts performed on the pendulum impact device. The results from the pendulum impact area fraction show a distinct break from the observed trend with the drop tower experiments. Rather than performance being strongly tied to sample thickness, doubling sample height here increased performance by < 10%. The performance/AF relationship likewise appears to be weaker, also varying by < 10% despite a doubling of AF between the sample types.

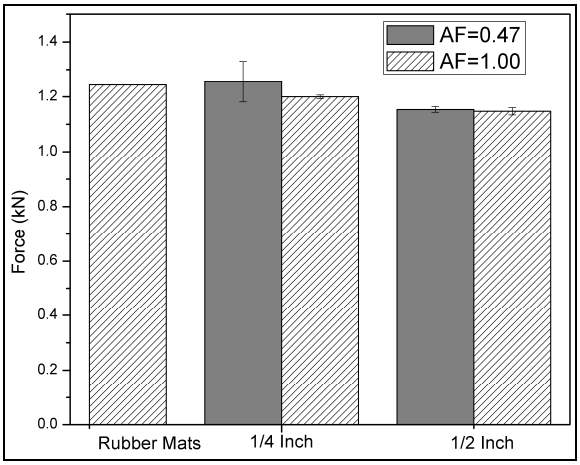

Figure 34: Area fraction results, femoral impact force, 25 J pendulum impact

The main advantage of higher area fraction appears to be less variability in performance, but not in overall performance. Also encouraging is the apparent re-distribution of energy during the impact due to the rotational motion. For each sample tested here, the peak impact force was < 1.5 kN. The best performing drop tower samples were 11 and 3.5 kN for ¼" and ½" samples respectively. The only concern with the results is that the simulated soft tissue alone protected nearly as well as the STF pad. The rubber mats also did not display the same fatiguing that the foam displayed as discussed in Chapter 4 making them candidates for a multiple use garment. The significantly lower peak forces were initially suspect despite the load

cell signal data being processing directly from manufacturer values. Other device sensors were checked to ensure other data produced expected values. A summary of this validation can be seen in Appendix F.

After testing, a complex bend was observed in the shaft part of the impact head. The energy of the impact caused it to bend in two places; the first bend was at the point where the shaft emerged from the impact head, the second was where the shaft emerged from the guiding piece attached to the pendulum arm. The bent impact head, seen in Figure 35, prevented further experiments from being performed.

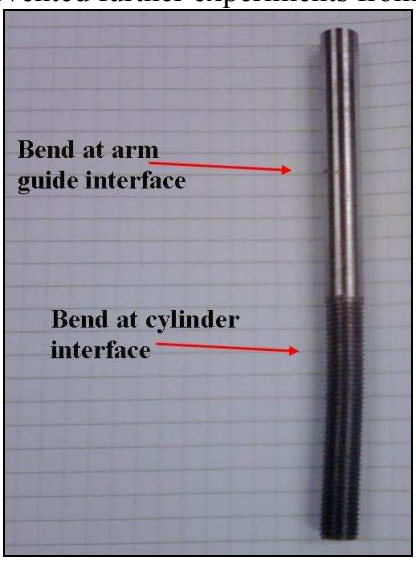

Figure 35: Complex bend on pendulum impact head after 25 J experiment

Naming the cause for the order of magnitude reduction in peak force proved difficult. Several possible contributing factors include the effect of rotational motion on the direction of fluid displacement. Another is the absorption of energy in motion by the arm in the x-y plane during impact.

The impact head was made with an adjustable shaft in order to allow the head to impact as close to parallel with the floor as possible. In addition to impact head's shaft bending, a slight twist was also observed after testing in the cross beam

which holds the load cell and weight bar. The cross bar itself was not bent, and was adjusted after testing was done via the braces holding it to the frame. Because of these small changes, and their resulting changes in the orientation of the head with respect to the sample, it is possible that the head could first contact the inner side (closest to the 'knee) of the sample and push fluid towards the outer side (farthest from the 'knee') giving the head a thicker than intended plug of fluid.

The force plates recorded forces in the x-y plane, as well as in the axial ('z') direction, during the impact. As seen in Figure 36, their peak values are significantly less than the femoral load cell.

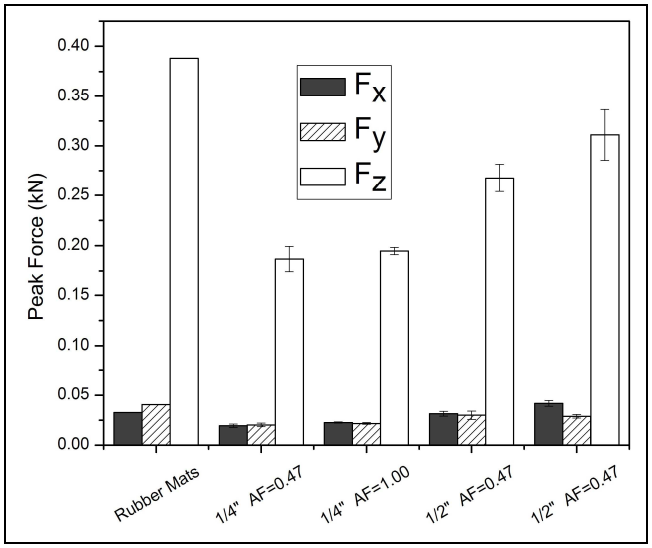

Figure 36: Force plate results, 25 J impact

Interestingly, the F_z value is 50-80% below the femoral force. Lower forces would be expected since the floor is essentially static, while the pendulum arm is being decelerated. F_x and F_y values are lower than F_z values by an order of magnitude which is also expected as the vast majority of the motion is in the axial direction at the moment of impact. The base of the pendulum machine was not observed to shift positions; energy absorbed as a result of these forces in the x-y direction would be too

small to explain the order of magnitude decrease in peak force from the drop tower experiment.

5.5 Area fraction conclusions

The peak force experienced during a vertical impact is strongly dependent on the area fraction of the STF in the protective garment. However, the marginal benefit to additional coverage diminishes around AF=0.50. Samples in this region performed as well as samples with area fractions of 1.00 to within 20%.

Impacts of the same energy, but carried out using a rotational motion decreased the peak force experienced by up to an order of magnitude for ¼" samples, and by a factor of 3 for ½" samples as compared to vertical motion. Increases in area fraction from 0.47 to 1.00 give only a 20% reduction in peak force, though variability between samples was lower at higher area fractions.

Regardless of the direction of motion the STF can now be dispersed in smaller plugs throughout a garment without the fear of decreased performance. Other benefits include decreased garment weight and increased flexibility during an impact.

Chapter 6

CONCLUSIONS

This study has shown that the favorable mechanical properties of shear thickening fluids can be used to improve the performance of various preventative medicine protective garments. Because of the energy dissipating viscous forces, both Newtonian and non-Newtonian fluids reduced peak forces by a factor of 2 over EVA foam at impact energies below 10 J.

STFs were found to perform better than Newtonian PDMS oils because STFs provided better resistance to flow. Impacts of oils typically resulted in the fluid plug squeezing to near zero height resulting in a spike in force as the impact head reached the sample platform. Discontinuously thickening STFs were found to perform better than continuously thickening despite the more rapid transition leading to more force being transmitted. When comparing impacts with four-fold increases in energy, discontinuous mixtures exhibited increases in peak forces of about 100%, for continuous mixtures, the jump was often well over 400%. The favored mixture became 45 vol. % Nanosil silica hard sphere particles dispersed in PEG200 because of favorable economics in addition to good performance.

Simulations of the impact experiments on Newtonian oils were done by approximating the fluid behavior as squeeze flow. The model correctly predicts trends for the Newtonian oils such as decreasing peak force with increasing viscosity. The model was expanded to help predict possible effects of the foam. EVA foam used as a

scaffold for the fluid plugs was found by the model to not significantly affect the peak force, nor was any foam with a Young's modulus below 0.1 MPa.

The marginal benefit of increased area fraction of STF in the pad was found to diminish above an area fraction of approximately 50%. On the drop tower, the difference in peak forces between the 50% and 100% area fraction samples was less than 20%. On the pendulum impact device, the difference was even less. Additionally, on the pendulum impact device, peak forces were decreased by an order of magnitude in ¼" samples with the best performing sample exhibiting peak forces of approximately 1.5 kN. The primary advantage of higher area fraction is less variability in peak force.

Chapter 7

FUTURE WORK

As discussed in Chapter 3, future garment testing could be avoided with improvements to the squeeze flow impact model shown for Newtonian fluids. The next step would be to expand the model for use with non-Newtonian fluids.

In order to test the viability of our best performing garment, the next experiment on the pendulum impact device would use the same STF pads described in Chapter 5 placed in series with the neoprene rubber. The impact would take place at the full 212 J predicted by Robinovitch *et al*. as the fall energy for an elderly female in the muscle relaxed state [15]. This would require the addition of 31 kg (~68 lbs) and increasing the drop height to about 0.7 meters. If the force experienced by the pendulum arm load cell is below 4.1 kN, then the garment should undergo further product development with regard to its carrier foam, and the strength of the sealant used to hold the foam and film together to increase the durability of the garment.

REFERENCES

[1] National Center for Injury Prevention and Control, Centers for Disease Control and Prevention (2010). Falls and hip fractures among older adults. Available online: http://www.cdc.gov/ncipc/factsheets/falls.htm (accessed April 1, 2010).

[2] WebMDHealth, Healthwise, Inc. Hip fracture. Available online: http://firstaid.webmd.com/tc/hip-fracture-topic-overview (accessed April 1, 2010).

[3] National Center for Injury Prevention and Control, Centers for Disease Control and Prevention (2010). The costs of fall injuries among older adults. Available online: http://www.cdc.gov/ncipc/factsheets/fallcost.htm (accessed April 1, 2010).

[4] Herseim, R. "DEVICE TO SIMULATE HIP IMPACT DURING HUMAN FALLS." Senior Thesis, University of Delaware. 2004.

[5] Robinovitch, S.N., Hayes, W.C., and McMahon, T.A.: Energy-shunting hip padding system attenuates femoral impact force in a simulated fall. Journal of Biomechanical Engineering, 117: 409-413, 1995.

[6] Kiel, D.P., Magaziner, J., Zimmerman, S., Ball, L., Barton, B.A., Brown, K.M., Stone, J.P., Dewkett, D., Birge, S.J. "Efficacy of a Hip Protector to Prevent Hip Fracture in Nursing Home Residents." Journal of the American Medical Association. 298, 4 (2007): 413-422.

[7] Juby, A.G. "The challenges of interpreting efficacy of hip protector pads in fracture prevention in high-risk seniors." Clinical Rheumatology. 28 (2009): 723-727.

[8] Warnke, A., Meyer, G., Bender, R., Mühlhauser, I. "Predictors of Adherence to the Use of Hip Protectors in Nursing Home Residents." Journal of the American Geriatric Society. 52, 3 (2004): 340-345.

[9] Kurrle, S.E., Cameron, I.D., Quine, S., Cumming, R.G. "Adherence with hip protectors: a proposal for standardised definitions." Osteoporosis International. 15 (2004): 1-4.

[10] Bender, J., Wagner, N.J. "Reversible shear thickening in monodisperse and bidisperse colloidal dispersions." Journal of Rheology. 40(5): 899-916 (1996).

[11] Kessler III, D., Dombrowski, R. Wagner, N., Kalman, D. "Testing the Hydrocluster Mechanism of Shear Thickening in Colloidal Dispersions - Measurements of the First Normal Stress Difference N_1." IACIS. Columbia, NY. June 2009.

[12] Egres, R. "THE EFFECTS OF PARTICLE ANISOTROPY ON THE RHEOLOGY AND MICROSTRUCTURE OF CONCENTRATED COLLOIDAL SUSPENSIONS THROUGH THE SHEAR THICKENING TRANSITION." University of Delaware, 2005.

[13] Engmann, J., Servais, C., Burbidge, A. "Squeeze flow theory and applications to rheometry: A review." Journal of Non-Newtonian Fluid Mechanics. (132) 2005: 1-27.

[14] Robinovitch, S.N. "Hip Fracture and Fall Impact Biomechanics." Massachusetts Institute of Technology. 1994.

[15] Robinovitch, S.N., Hayes, W.C., and McMahon, T.A. "Prediction of femoral impact forces in falls on the hip." Journal of Biomechanical Engineering. 117: 366-374.

[16] Burstein, A.H., Reilly, D.T., Martens, M. "Aging of bone tissue: mechanical properties." Journal of Bone Surgery (American). 58, 1 (1976): 82-86.

[17] McCalden, R.W., McGeough, J.A., Barker, M.B., *et al.* "Age-related changes in tensile properties of cortical bone. The relative importance of changes in porosity, mineralization, and microstructure." Journal of Bone Surgery (American). 75, 8 (1993): 1193-1205.

[18] Zioupos, P., Currey, J.D. "Changes in the stiffness, strength, and toughness of human cortical bone with age." Bone. 22, 1 (1998): 57-66.

[19] Roberts, B.J., Thrall, E., Muller, J.A., Bouxsein, M.L. "Comparison of hip fracture risk prediction by femoral aBMD to experimentally measured factor of risk." Bone. 46 (2010): 742-746.

[20] Courtney, A.C., Wachtel, E.F., Myers, E.R., *et al.* "Age-related reductions in the strength of the femur tested in a fall-loading configuration." Journal of Bone Surgery (American). 77, 3 (1995): 387-395.

[21] Dombrowski, R.D. "Rheology of shear thickening fluids." Unpublished data, 2009.

[22] Dombrowski, R., Swanik, C.S., Wagner, N.J. "Final Report: Development and testing of STF hip pad." Unpublished data. 2008.

[23] Dynatup® Drop Weight Impact Test Machine. Instron. Available online: www.instron.co.uk/wa/library/streamFile2.aspx?sdoc=367 (accessed May 9, 2010).

[24] Stefan, J., "Versuche über die scheinbare Adhäsion" Sitzungsberichte der Kaiserlichen Akademie der Wissenschaften in Wien. 69 (2): 713–735. (1874). (Qtd in. Engmann *et al*.)

[25] Kuzma, D. "Fluid Inertia Effects In Squeeze Films." Applied Scientific Research. (18) 1968. 15-20.

[26] Leider, P.J., Bird, R.B. "Squeezing flow between parallel disks: I. Theoretical analysis." Industrial and Engineering Chemistry Fundamentals. 13 (1974) 336–341. (Qtd in. Engmann *et al*.)

[27] University of Birmingham, Polymer Engineering Research Group. Polymer Foam Case Studies. Available online: http://www.foamstudies.bham.ac.uk/index.htm (accessed April 1, 2010).

Appendix A

DERIVATION OF DIFFERENTIAL EQUATIONS FOR SQUEEZE FLOW SIMULATIONS IN MATLAB

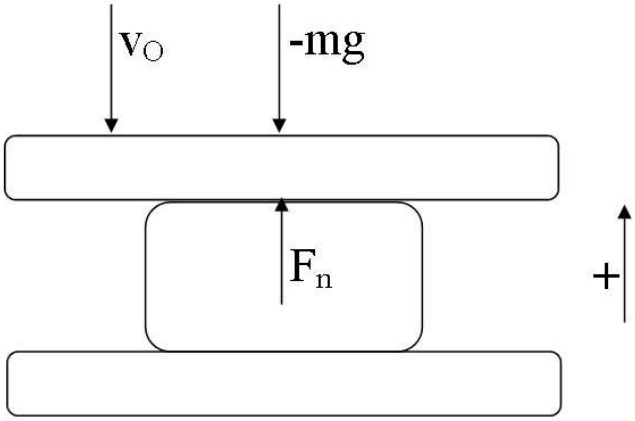

$$F = F_n - mg$$

$$ma = F_n - mg$$

Differential equation 1: $\boxed{\frac{dv}{dt} = a = \frac{F_n}{m} - g}$

Differential equation 2: $\boxed{\frac{dx}{dt} = v}$

Post processing, F_n can be calculated by differentiating velocity data to obtain acceleration, and then solving differential equation 1 in reverse.

Appendix B

MATLAB CODE FOR NEWTONIAN OIL SQUEEZE FLOW SIMULATIONS

The code incorporating the differential equations was written in the function file "NewtonNoSlip" seen below.

```
function dy = NewtonNoSlip(t, y)

global mu radius mass

dy = zeros(2, 1);
dy(1) = y(2); %y(1) is position, y(2) is velocity
dy(2) =(-3*pi*mu*((radius)^4)*(y(2)))/(2*mass*((y(1))^3))-9.8;
```

The script file solved these equations given a user defined viscosity, initial plug thickness and radius, the initial speed of the top plate (same as impact speed), and the mass of the top plate. The values currently entered mimic a 1 m/s impact of a ¼" thick, 1" diameter target with a viscosity of 480 Pa.s with the minimum mass allowed by the drop tower. After the differential equation function has run, the normal force is calculated using acceleration data, and displacement is calculated based on position data and initial height.

```
clear all;
close all;

global mu radius mass

mu=480; %28.8, 96, 480
radius=0.0127; %1 in D, .5 in radius
%radius=0.0047625; %3/8 in D
mass=3.55;

tspan = [0:.0001:.01];
%Ho=0.009525; %3/8 in foam
Ho=0.00635; %1/4 in foam
Vo=-1.00;
IC = [Ho; Vo];
```

```
[T, Y] = ode45(@NewtonNoSlip, tspan, IC);

i=1;
for i=1:(length(T)-1)
    a=(Y(i+1,2)-Y(i,2))/(T(i+1)-T(i));
    force(i,1)=(a+9.8)*mass;
end
force(length(T),1)=force(length(T)-1,1);

plot(T, force)
xlabel('time');
ylabel('force (N)');

for i=1:length(T)
    disp(i,1)=Ho-Y(i,1);
end

for i=1:length(T)
    all(i,1)=T(i,1)*1000;
    all(i,2)=disp(i,1)*1000;
    all(i,3)=force(i,1)/1000;
    all(i,4)=Y(i,2);
end
figure()
plot(disp,force)
axis([0 Ho 0 3000]);
```

Appendix C

DERIVATION OF FOAM SPRING FORCE FOR COMBINED FOAM/FLUID SQUEEZE FLOW MODEL

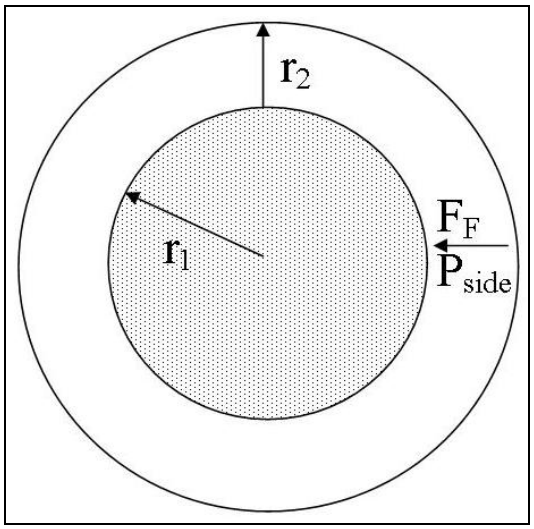

In this model, there is a fluid (shaded) plug of radius r_1 surrounded by a foam ring (blank) with a thickness or r_2. Note that r_2 is not a radius, but rather a difference in radii. When the fluid is impacted, it is compressed axially, and expands radially. The foam ring impedes this radial expansion as a Hookean spring exerting a pressure (P_{side}) along the outside of the plug. The force exerted by the side of the foam (F_F) was assumed to act in series to the normal force on the impact head created by the fluid.

The additional pressure at the top was said to be equivalent to the foam force divided by the contact area: $P_{top} = \frac{F_F}{\pi(r_{1,o}^2)}$

The pressure exerted by the foam could be solved for using the stress-strain equation:

$P_{side} = E\varepsilon = E\dfrac{\left(r_1 - r_{1,0}\right)}{r_{2,o}}$ where $\varepsilon = \dfrac{\Delta r}{r} = \dfrac{\left(r2 - r_{2,0}\right)}{r_{2,o}} = \dfrac{\left(r_1 - r_{1,0}\right)}{r_{2,o}}$.

Setting the two pressures equal, the following equation for F_F is obtained:

$F_F = \dfrac{\pi E r_{1,o}^2 (r_1 - r_{1,o})}{r_{2,o}}$ which simplifies to $F_F = \pi E r_{1,o}(r_1 - r_{1,o})$ if the thickness of the foam ring is assumed to be the same as the radius of the plug. This is a reasonable assumption for a garment that is about 50% fluid.

In order to calculate this force as part of the differential equation set discussed in Appendix A we have to relate plug height and plug radius using conservation of mass:

$m_o = \rho V_o = \rho V = m$

The volume of the plug can be written: $V = \pi r^2 h$

Given constant density, plug radius can be rewritten as $r_1 = r_{1,o}\sqrt{\dfrac{h_o}{h}}$

Substituting this into the equation for F_F, the equation can be re-written and simplified to the final form: $F_F = \pi E r_{1,o}^2\left(\sqrt{\dfrac{h_o}{h}} - 1\right)$

This force was placed in the model described in Appendix A acting in series with the normal force.

Appendix D

SAMPLE WEIGHTS AND PEAK FORCES FROM FLUID SELECTION EXPERIMENTS

	Date	Sample	Thickness (inch)	Filling	Energy (J)	Peak Force (kN)	Fluid Weight (g)
Newtonian	1/23/2009	Sample1	1/4	28.8 Pa.s	1.78	2.25	3.01
		Sample2	1/4	28.8 Pa.s	1.78	2.09	2.85
		Sample3	1/4	28.8 Pa.s	1.78	2.13	2.83
		Sample4	1/4	96 Pa.s	1.78	1.70	2.9
		Sample5	1/4	96 Pa.s	1.78	1.52	3.03
		Sample6	1/4	96 Pa.s	1.78	1.50	2.95
		Sample7	1/4	480 Pa.s	1.78	1.25	2.81
		Sample8	1/4	480 Pa.s	1.78	1.33	2.8
		Sample9	1/4	480 Pa.s	1.78	1.12	2.9
	6/30/2009	Sample1	1/2	28.8 Pa.s	1.78	3.11	5.6
		Sample2	1/2	28.8 Pa.s	1.78	2.95	6.31
		Sample3	1/2	28.8 Pa.s	1.78	3.10	6.23
		Sample4	1/2	28.8 Pa.s	7.1	9.35	5.58
		Sample5	1/2	28.8 Pa.s	7.1	9.40	6.03
		Sample6	1/2	28.8 Pa.s	7.1	9.39	5.96
		Sample7	1/2	96 Pa.s	1.78	3.09	5.71
		Sample8	1/2	96 Pa.s	1.78	2.47	6.24
		Sample9	1/2	96 Pa.s	1.78	3.00	5.87
		Sample10	1/2	96 Pa.s	7.1	9.41	5.89
		Sample11	1/2	96 Pa.s	7.1	9.43	5.83
		Sample12	1/2	96 Pa.s	7.1	9.41	6.15
		Sample13	1/2	480 Pa.s	1.78	3.01	5.85
		Sample14	1/2	480 Pa.s	1.78	2.95	5.81
		Sample15	1/2	480 Pa.s	1.78	2.97	6.21
		Sample16	1/2	480 Pa.s	7.1	9.36	6.1
		Sample17	1/2	480 Pa.s	7.1	9.35	5.94
		Sample18	1/2	480 Pa.s	7.1	9.35	5.87

STF	1/27/2009	Sample1	1/4	52 vol.% Shokubai	1.78	3.14	4.73
		Sample2	1/4	52 vol.% Shokubai	1.78	3.02	4.40
		Sample3	1/4	52 vol.% Shokubai	1.78	3.05	4.63
		Sample4	1/4	52 vol.% Shokubai	7.1	3.89	4.57
		Sample5	1/4	52 vol.% Shokubai	7.1	4.22	4.53
		Sample6	1/4	52 vol.% Shokubai	7.1	3.96	4.67
	7/2/2009	Sample6	1/4	25 wt.% Cabosil	1.78	0.65	4.00
		Sample7	1/4	25 wt.% Cabosil	1.78	0.57	4.23
		Sample8	1/4	25 wt.% Cabosil	1.78	0.61	3.86
		Sample12	1/4	45 vol.% Nanosil	1.78	1.41	3.67
		Sample13	1/4	45 vol.% Nanosil	1.78	1.38	3.52
		Sample14	1/4	45 vol.% Nanosil	1.78	1.43	3.68
		Sample16	1/4	45 vol.% Nanosil	7.1	2.50	3.81
		Sample17	1/4	45 vol.% Nanosil	7.1	2.35	4.01
		Sample18	1/4	48 vol.% Shokubai	1.78	1.44	4.61
		Sample19	1/4	48 vol.% Shokubai	1.78	1.28	4.66
		Sample20	1/4	48 vol.% Shokubai	1.78	0.75	4.96
		Sample21	1/4	48 vol.% Shokubai	7.1	3.52	5.19
		Sample22	1/4	48 vol.% Shokubai	7.1	3.06	5.11
		Sample23	1/4	48 vol.% Shokubai	7.1	3.04	5.21
	7/9/2009	Sample7	1/4	25 wt.% Cabosil	7.1	3.75	5.19
		Sample8	1/4	25 wt.% Cabosil	7.1	3.22	5.79
		Sample9	1/4	25 wt.% Cabosil	7.1	3.56	5.25
	7/28/2009	Sample1	1/2	48 vol.% Shokubai	1.78	2.43	9.25
		Sample2	1/2	48 vol.% Shokubai	1.78	2.43	9.13
		Sample3	1/2	48 vol.% Shokubai	1.78	2.40	9.58
		Sample4	1/2	48 vol.% Shokubai	7.1	7.59	9.23
		Sample5	1/2	48 vol.% Shokubai	7.1	7.62	9.41
		Sample6	1/2	48 vol.% Shokubai	7.1	7.63	9.38
		Sample7	1/2	25 wt.% Cabosil	1.78	2.16	7.35
		Sample8	1/2	25 wt.% Cabosil	1.78	2.16	7.33
		Sample9	1/2	25 wt.% Cabosil	1.78	2.17	7.21
		Sample10	1/2	25 wt.% Cabosil	7.1	7.53	7.11
		Sample11	1/2	25 wt.% Cabosil	7.1	7.44	7.40
		Sample12	1/2	25 wt.% Cabosil	7.1	7.45	7.38
	7/30/2009	Sample1	1/2	52 vol.% Shokubai	1.78	1.58	9.64
		Sample2	1/2	52 vol.% Shokubai	1.78	1.47	9.45
		Sample3	1/2	52 vol.% Shokubai	1.78	1.44	9.76
		Sample4	1/2	52 vol.% Shokubai	7.1	1.74	8.55
		Sample5	1/2	52 vol.% Shokubai	7.1	1.79	9.47
		Sample6	1/2	52 vol.% Shokubai	7.1	1.75	9.69

Appendix E

SAMPLE WEIGHTS AND PEAK FORCES FROM AREA FRACTION EXPERIMENTS

	Date	Sample	Thickness (inches)	AF	Peak Force (kN)	Fluid Weight (g)
Drop Tower	1/27/2010	Sample1	1/4	0.33	21.14	5.46
		Sample2	1/4	0.33	20.68	5.33
		Sample3	1/4	0.33	21.84	5.36
		Sample4	1/4	1.00	11.27	5.30
		Sample5	1/4	1.00	10.27	5.34
		Sample6	1/4	1.00	10.56	5.33
		Sample7	1/2	0.33	8.97	10.43
		Sample8	1/2	0.33	9.38	9.66
		Sample9	1/2	0.33	11.08	10.39
		Sample10	1/2	1.00	3.38	11.04
		Sample11	1/2	1.00	3.64	9.96
		Sample12	1/2	1.00	3.35	10.27
	2/4/2010	Sample1	1/4	0.47	14.46	6.06
		Sample2	1/4	0.47	14.16	6.14
		Sample3	1/4	0.47	13.92	5.83
		Sample4	1/2	0.47	5.95	11.94
		Sample5	1/2	0.47	4.55	12.68
		Sample6	1/2	0.47	4.44	12.62
		Sample7	1/2	1.00	3.79	10.33
		Sample8	1/2	1.00	4.08	10.35
		Sample9	1/2	1.00	3.64	10.64
		Sample10	1/4	1.00	11.68	5.34
		Sample11	1/4	1.00	11.33	5.22
		Sample12	1/4	1.00	11.12	5.23
	2/2/2010	Sample1	1/4	0.47	10.85	5.14
		Sample2	1/4	0.47	11.59	5.41
		Sample3	1/4	0.47	11.50	5.09
		Sample4	1/2	0.47	6.19	10.77
		Sample5	1/2	0.47	6.16	10.75
		Sample6	1/2	0.47	6.30	9.01

Pendulum	3/26/2010	Sample1	1/4	0.47	0.17	4.74
		Sample2	1/4	0.47	0.20	4.85
		Sample3	1/4	0.47	0.19	4.69
		Sample4	1/4	1.00	0.20	5.60
		Sample5	1/4	1.00	0.20	5.09
		Sample6	1/4	1.00	0.19	5.06
		Sample7	1/2	0.47	0.27	9.93
		Sample8	1/2	0.47	0.25	9.49
		Sample9	1/2	0.47	0.28	9.78
		Sample10	1/2	1.00	0.31	11.34
		Sample11	1/2	1.00	0.34	10.85
		Sample12	1/2	1.00	0.29	11.15

Appendix F

PENDULUM IMPACTOR KINEMATIC DATA FROM 25 J EXPERIMENT FOR VALIDATION OF THE DEVICE

The figure shown below contains the position, velocity, and acceleration data for a 25 J impact of a ½" thick 45 vol. % Nanosil sample with an area fraction of 1.00.

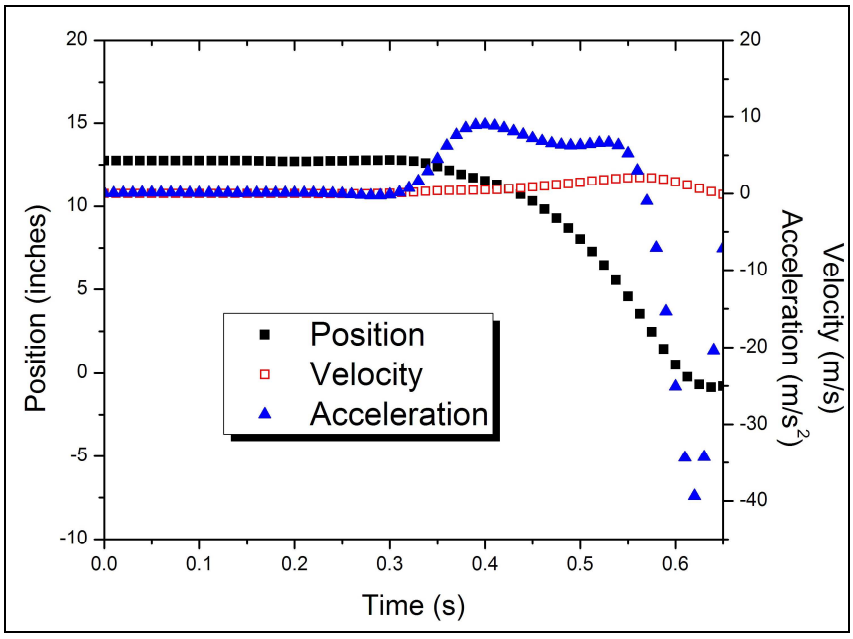

The position data dips below zero because the zero point was not set for the machine. The difference in the initial and final position is about 14". The drop height had been set by a manual measurement to about 13", from the impact head to the top of the sample, to reach the correct impact speed. This did not account for the compression of the sample. The resolution of the potentiometer is approximately 1 mm.

The velocity increases gradually after the arm is released at approximately 0.3 seconds, and increases to the impact speed of 2.1 m/s at about 0.55 seconds. During this time, the acceleration jumps from close to zero to slightly below 10 m/s^2. The expected acceleration of free fall is 9.8 m/s^2 assuming linear motion and no friction. In this case, the motion is rotational, making the acceleration slightly less than 9.8 m/s^2. Acceleration spikes downward upon impact, as expected, and becomes positive again during a subsequent bounce.